METHODOLOGY – Review Article

Chemical Exchange Saturation Transfer (CEST): What is in a Name and What Isn't?

Peter C. M. van Zijl,[1,2]* and Nirbhay N. Yadav[1,2]

Chemical exchange saturation transfer (CEST) imaging is a relatively new magnetic resonance imaging contrast approach in which exogenous or endogenous compounds containing either exchangeable protons or exchangeable molecules are selectively saturated and after transfer of this saturation, detected indirectly through the water signal with enhanced sensitivity. The focus of this review is on basic magnetic resonance principles underlying CEST and similarities to and differences with conventional magnetization transfer contrast. In CEST magnetic resonance imaging, transfer of magnetization is studied in mobile compounds instead of semisolids. Similar to magnetization transfer contrast, CEST has contributions of both chemical exchange and dipolar cross-relaxation, but the latter can often be neglected if exchange is fast. Contrary to magnetization transfer contrast, CEST imaging requires sufficiently slow exchange on the magnetic resonance time scale to allow selective irradiation of the protons of interest. As a consequence, magnetic labeling is not limited to radio-frequency saturation but can be expanded with slower frequency-selective approaches such as inversion, gradient dephasing and frequency labeling. The basic theory, design criteria, and experimental issues for exchange transfer imaging are discussed. A new classification for CEST agents based on exchange type is proposed. The potential of this young field is discussed, especially with respect to in vivo application and translation to humans. Magn Reson Med 65:927–948, 2011. © 2011 Wiley-Liss, Inc.

Key words: MRI; chemical exchange; magnetization transfer; contrast agent; dipolar transfer

INTRODUCTION

When using contrast agents in magnetic resonance imaging (MRI), the requirements are pretty much the same as for any other imaging modality, namely generating the desired contrast while using the lowest possible concentration of agent to avoid perturbing the physiological environment and to minimize toxicity. Due to inherent limitations in sensitivity, MRI has a great disadvantage compared to optical and radioactive methods in that high concentrations of contrast agent are required. To make matters worse, most of the (super)paramagnetic metals used to enhance relaxation are toxic when not chelated or coated. This limitation of exogenous MRI contrast to relaxation agents was the status quo until 2000, when Ward and Balaban (1) suggested using exchangeable protons for MRI contrast, which extended the range of possible MR agents to include diamagnetic compounds. They demonstrated the possibility to turn this contrast on and off by using selective radiofrequency (RF) saturation of the protons of interest and named this approach "chemical exchange saturation transfer" or "CEST." Recently, many outstanding reviews (2–11) have been published summarizing the CEST literature with respect to theory and application. To avoid too much repetition, we focus on the basic MR principles underlying CEST (what's in the name) and its similarities to and differences with conventional magnetization transfer contrast [MTC, (12)] used in the clinic, which is based on irradiation of protons in immobile semisolid macromolecules (such as bound proteins, membranes, and myelin). We also critically review many experimental pitfalls underlying the current CEST approach, the interference of competing MT mechanisms (what's not in the name), and some promising approaches that allow the study of exchange transfer without the need for RF saturation.

CEST Mechanism

The underlying principles of CEST imaging are very simple (Fig. 1a): exchangeable solute protons (s) that resonate at a frequency different from the bulk water protons (w) are selectively saturated using RF irradiation.[1] This saturation is subsequently transferred to bulk water when solute protons exchange with water protons (exchange rate k_{sw}) and the water signal becomes slightly attenuated. In view of the low concentration of solute protons (μM to mM range), a single transfer of saturation would be insufficient to show any discernable effect on water protons, the concentration of which is about 110 M. However, because the water pool is much larger than the saturated solute proton pool, each exchanging saturated solute proton is replaced by a nonsaturated water proton, which is then again saturated. If the solute protons have a sufficiently fast exchange rate (residence time in millisecond range) and the saturation time (t_{sat}) is sufficiently long (second range), prolonged irradiation leads to substantial enhancement of this saturation effect, which eventually becomes visible on the water

[1]The Russell H. Morgan Department of Radiology and Radiological Science, Division of MR Research, The Johns Hopkins University School of Medicine, Baltimore, Maryland, USA.

[2]F.M. Kirby Research Center for Functional Brain Imaging, Kennedy Krieger Institute, Baltimore, Maryland, USA.

Grant sponsor: NIH-NCRR; Grant number: P41-RR15241.

*Correspondence to: Peter C. M. van Zijl, Ph.D., Johns Hopkins University School of Medicine, Dept. of Radiology, 217 Traylor Bldg, 720 Rutland Ave., Baltimore, MD 21205. E-mail: pvanzijl@mri.jhu.edu

Received 22 September 2010; revised 1 November 2010; accepted 24 November 2010.

DOI 10.1002/mrm.22761
Published online 17 February 2011 in Wiley Online Library (wileyonlinelibrary.com).

[1]RF saturation refers to equilibrating the populations of the proton energy levels, which is difficult to achieve fully for times $< 5T_1$. Often, only partial saturation can be achieved, especially when exchange rates are fast (see theory section for saturation efficiency).

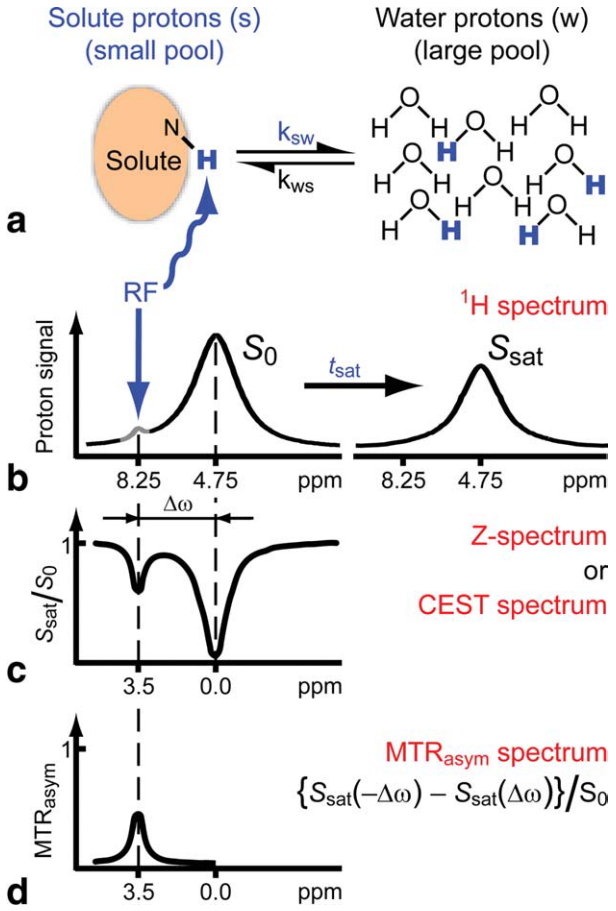

FIG. 1. Chemical exchange saturation transfer (CEST): principles and measurement approach for pure exchange effects. **a, b:** Solute protons (blue) are saturated at their specific resonance frequency in the proton spectrum (here 8.25 ppm for amide protons). This saturation is transferred to water (4.75 ppm) at exchange rate k_{sw} and nonsaturated protons (black) return. After a period (t_{sat}), this effect becomes visible on the water signal (b, right). **c:** Measurement of normalized water saturation (S_{sat}/S_0) as a function of irradiation frequency, generating a so-called Z-spectrum (or CEST spectrum or MT spectrum). When irradiating the water protons at 4.75 ppm, the signal disappears due to direct (water) saturation (DS). This frequency is assigned to 0 ppm in Z-spectra. At short saturation times, only this direct saturation is apparent. At longer t_{sat} the CEST effect becomes visible at the frequency of the low-concentration exchangeable solute protons, now assigned to 8.25 − 4.75 = 3.5 ppm in the Z-spectrum. **d:** result of magnetization transfer ratio (MTR = 1 – S_{sat}/S_0) asymmetry analysis of the Z-spectrum with respect to the water frequency to remove the effect of direct saturation. In the remainder of this article we will use the standard NMR chemical shift assignment for water at 4.75 ppm in ^{1}H spectra, while the 0 ppm assignment will be used in Z-spectra. [Color figure can be viewed in the online issue, which is available at wileyonlinelibrary.com.]

signal (Fig. 1b), allowing the presence of low-concentration solutes to be imaged indirectly. These frequency-dependent saturation effects are visualized similar to conventional MT spectra by plotting the water saturation (S_{sat}) normalized by the signal without saturation (S_0) as a function of saturation frequency (Fig. 1c). This gives what has been dubbed a Z-spectrum (13) or CEST spectrum. Such a spectrum is characterized by the symmetric direct saturation (DS) around the water frequency, which has led to assignment of 0 ppm to the water frequency, a feature confusing for basic NMR spectroscopists. This DS may interfere with detection of CEST effects, which is addressed by employing the symmetry of the DS through a so-called MT ratio (MTR) asymmetry analysis (14) with respect to the water frequency (Fig. 1d). Such an analysis inherently assumes independent contributions of solute and water protons, which need not be the case, but it works well as a first approximation. Using the literature definition of MT ratio (MTR = 1 − S_{sat}/S_0), this process is characterized by subtracting right (−Δω) and left (Δω) signal intensity ratios through (14):

$$\begin{aligned} \mathrm{MTR}_{asym}(\Delta\omega) &= \mathrm{MTR}(\Delta\omega) - \mathrm{MTR}(-\Delta\omega) \\ &= S_{sat}(-\Delta\omega)/S_0 - S_{sat}(\Delta\omega)/S_0, \end{aligned} \quad [1]$$

in which Δω is the frequency difference with water. Similar to MT imaging, it has to be realized that this type of quantification is often difficult to reproduce between laboratories because, unless saturation efficiency is 100%, the effect depends on strength of the applied RF field (B_1), generally referred to as power in MR jargon. This can be somewhat ameliorated by taking left/right ratios of the signal attenuation, but doing this complicates quantification in terms of exchange rates and concentrations. Asymmetry analysis also is based on an inherent assumption of symmetry of non-CEST contributions around the water signal, which often is incorrect, especially in vivo but also in vitro.

Theoretical Description and Spectral Features

The CEST effect is generally expressed in terms of a signal reduction (S_{sat}/S_0 or M_s/M_0 for magnetization), which is then converted to MTR$_{asym}$. However, these are experimentally measured quantities that may have multiple effects contributing (see "Signal and Parameter Quantification" section). As most CEST work relates to protons, we will describe the pure exchange transfer effect in a manner normalized per proton using a so-called proton transfer ratio (PTR), which can be compared for all different mechanisms. Thus, if the measured MTR$_{asym}$ would be caused purely by exchange, it would equal PTR. For a complete description of the exchange process that would be valid at any exchange rate, it is necessary to use the Bloch equations (15–23). Using a two-pool exchange model (small solute pool and large water pool, no back exchange of saturated protons) a simple analytical solution providing PTR in the steady state can be derived under the assumption that RF irradiation of the solute pool does not perturb the water pool [i.e., no spillover (18,23)]:

$$\mathrm{PTR} = x_s \cdot \alpha \cdot k_{sw} \cdot T_{1w}\left(1 - e^{-t_{sat}/T_{1w}}\right), \quad [2]$$

in which

$$x_s = \frac{[\text{exchangeable proton}]}{[\text{water proton}]} = \frac{k_{ws}}{k_{sw}}. \quad [3]$$

Square brackets indicate concentration. Thus, the measured CEST effect increases with the fractional concentration of the solute protons x_s, the saturation efficiency α, and the exchange rate k_{sw}, while being counteracted by the longitudinal relaxation rate ($1/T_{1w}$) of water. It

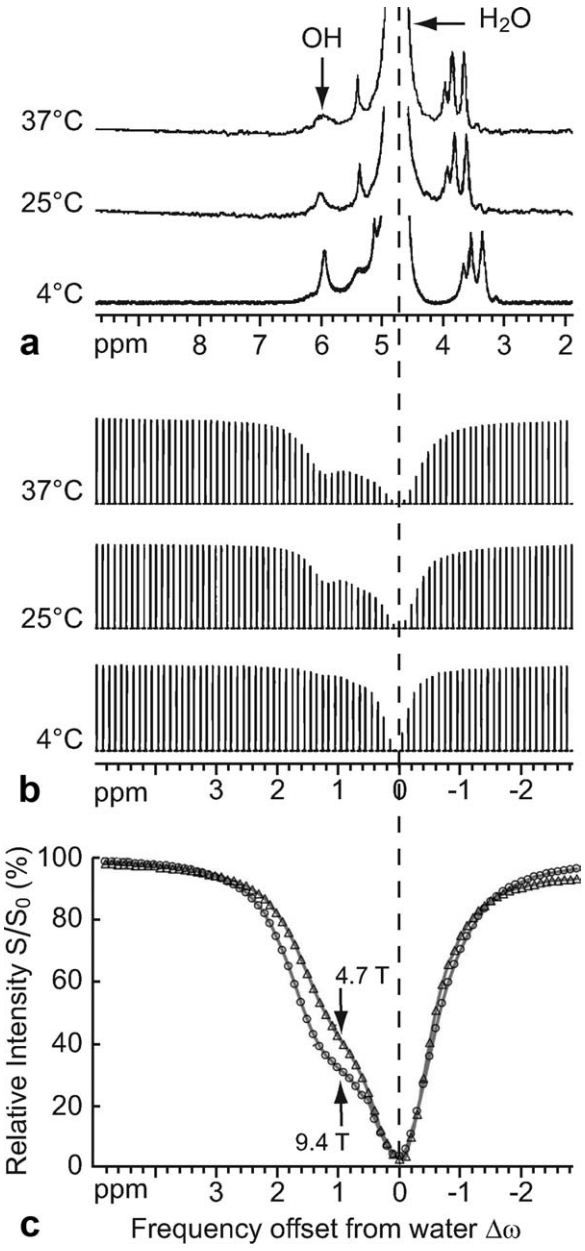

FIG. 2. Effect of exchange regime on proton spectra versus CEST spectra for a solution of 200 mM glycogen. **a:** ^{1}H NMR spectra acquired at 9.4 T in unbuffered H_2O (pH = 7) as a function of temperature. The OH resonances at 1.2 ppm and 0.7 ppm (2:1 ratio) from water broaden at higher temperature, where exchange is faster. **b:** The corresponding CEST-spectra show increased glycogen detectability at higher temperature. **c:** CEST-spectra in PBS buffer (37°C, pH = 7.4) acquired at 9.4 T and 4.7 T using t_{sat} = 10 s, B_1 = 1.9 μT. Notice the better definition of the CEST effect at higher field due to the increased chemical shift difference with water. Reproduced with permission from van Zijl et al., Proc Natl Acad Sci USA 2007;104:4359–4364.

should be pointed out that T_{1w} is the T_1 of water measured without saturation, because, similar to most MR relaxation parameters, measurement of T_1 may depend on the pulse sequence used. For instance, when tissue T_1 is determined using saturation ($T_{1w,sat}$) it will appear different from T_{1w} because there are contributions from exchange. The CEST effect is expected to increase at higher field, because T_{1w} increases with field strength, allowing prolonged storage of saturation in the water pool. However, the two T_{1w} terms counteract each other and, for constant t_{sat}, the expected increase is only about 8% from 1.5 to 3 T and 9% from 3 to 7 T, which may not be worth the trouble in view of the large increases in power deposition with the square of the field. The main advantage at high field is the frequency separation in terms of better adherence to the slow-exchange condition and reduced interference of direct water saturation, which will be discussed later.

For mobile solutes, neglecting transverse relaxation, the saturation efficiency can be approximated by (18,23,24):

$$\alpha \approx \frac{(\gamma B_1)^2}{(\gamma B_1)^2 + (k_{sw})^2}. \quad [4]$$

Therefore, rapidly exchangeable protons can only be saturated efficiently by applying more RF power, which is disadvantageous in vivo due to specific absorption rate (SAR) requirements. This situation is still favorable when studying the amide protons in the peptide bonds of small tissue proteins and peptides, as they exchange with a rate of about 29 Hz (23,25), for which a typical irradiation field (B_1) of 1 μT (γB_1 = 267.5 rad s^{-1}) on a human scanner leads to α = 0.99. However, for contrast agents studied at low concentration, where high exchange rates are needed to visualize any effect, or for the rapidly exchanging water molecules in paramagnetic (paraCEST) agents, power deposition may become a problem when using continuous saturation.

The need to selectively saturate the solute protons appears to require the condition of slow exchange ($\Delta\omega >> k_{sw}$) on the MR time scale to be fulfilled. CEST technology definitely becomes more applicable at higher magnetic fields as the shift difference in Hz increases proportional to field strength. Compared to conventional NMR, however, the CEST approach has a great advantage in that it is not a requirement for the exchangeable proton resonance of interest to be clearly visible in the NMR spectrum to allow detection via saturation transfer. This principle is illustrated in Fig. 2 for glycogen at a field of 9.4 T. Glycogen is a glucose polymer that is highly abundant in liver and muscle, and contains multiple OH groups resonating in the range of 0.5–1.5 ppm ($\Delta\omega$ = 630–1890 rad s^{-1}) from water. Exchange is intermediate on the MR time scale at this field strength and, due to excessive broadening, the hydroxyl protons are not visible in a standard proton spectrum under buffered physiological conditions (pH ~ 7.1–7.3; temperature ~ 37°C). However, in water without buffer, NMR detection is possible. Figure 2a shows high-resolution ^{1}H NMR spectra of glycogen (200 mM concentration per glucose unit) in water as a function of temperature with resonances at 0.7 and 1.2 ppm downfield from water, assigned to the two OH ring protons (C2, C3) and the CH_2OH sidegroup (C6), respectively (26). The linewidth of the —OH resonance at 1.2 ppm gradually broadens when increasing the temperature from 4 to 37 °C, characteristic of —OH protons in relatively slow exchange with free water protons. Interestingly, while the temperature-based increase in —OH exchange rate reduces

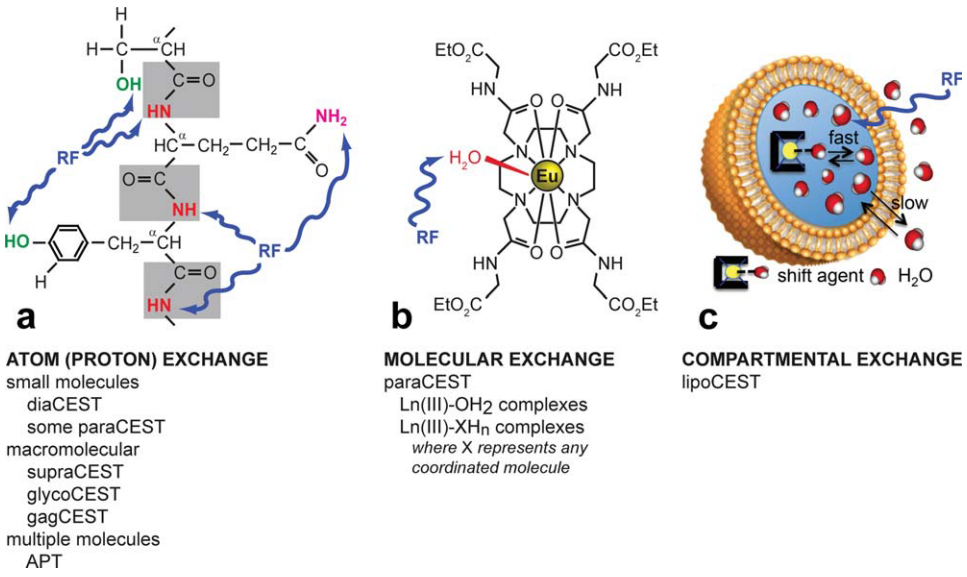

FIG. 3. Classification of CEST contrast based on exchange type. **a:** Proton exchange: magnetic labeling of exchangeable protons, which is the case for most diamagnetic CEST (DIACEST) compounds reported until now and several paramagnetic (PARACEST) agents. As an example, hydroxyl, amide and amine protons in a peptide are shown. SupraCEST relates to paramagnetic agents that are coordinated to macromolecular units in which the exchangeable side group protons are studied (113). **b:** Molecular exchange: magnetic labeling of exchangeable molecules, in this case a water molecule coordinated to Europium in a PARACEST agent. For these agents, the molecular exchange rate is generally faster than the proton–proton exchange rate (Courtesy of Dr. Mark Woods, Portland State University, Portland). **c:** Compartmental exchange: Magnetic labeling of compartmentalized water molecules in a fast-exchange environment resulting in a single average resonance frequency for compartmental water that is different from bulk water. This shift can be induced by either a paramagnetic or diamagnetic agent locked into the compartment or by changing the shape of the compartment to induce a bulk magnetic susceptibility (BMS) anisotropy. The shift difference allows selective irradiation of the compartmental pool. Due to the large size of the irradiated water pool and the fact that the effect spreads beyond the liposome, giga-size enhancements can be induced (Table 1). [Color figure can be viewed in the online issue, which is available at wileyonlinelibrary.com.]

visibility in the proton NMR spectra (Fig. 2a), the detection sensitivity is enhanced in the CEST-spectra (Fig. 2b) due to the dependency of the CEST effect on the proton exchange rate (Eq. 2). When using a glycogen solution in PBS buffer at physiological pH, the exchange rate increases dramatically, but CEST effects are still visible in the Z-spectra (Fig. 2c), indicating that sufficient saturation can be achieved within the brief lifetime of the hydroxyl protons on the glycogen. As expected, the detectability reduces at lower magnetic field (Fig. 2c).

CEST Classifications and Proton Transfer Efficiencies

CEST constitutes a powerful sensitivity enhancement mechanism in which low concentration solutes can be visualized through the water signal. The enhancement depends on the agent proton concentration (Eq. 2) and the rate of exchange (Eqs. 2 and 3), allowing the specific design of agents, constructs, and MRI pulse sequences to optimize the contrast based on these two parameters. CEST is therefore inherently suitable as a molecular and cellular imaging approach and can employ both paramagnetic (2,27–30) and diamagnetic species (1,24,25,31–33), which has led to the nomenclature of paraCEST (2) and diaCEST (4), respectively. This useful classification relates mostly to the size of the chemical shift difference with water, which can be enlarged tremendously when using paramagnetic shift agents, thereby allowing much higher exchange rates to be used while still adhering to the slow-intermediate MR exchange regime. For diaCEST compounds the range is generally 0–7 ppm from water (hydroxy, amine, amide, and imino groups), but this can be extended to 18 or 19 ppm through hydrogen bonding. With respect to nomenclature, early classifications have been made in terms of molecular size, endogenous occurrence and type of molecular construct (10,11). In addition, many approaches have been named specifically for the proton, molecule, or mechanism involved by adding CEST to the name, e.g., glycoCEST for glycogen (26), gagCEST for glycosaminoglycans (34), lipoCEST for liposomes (35). However, there is overlap between the classes as both macromolecular and liposome applications exist for paraCEST and diaCEST agents and many of the same approaches can be applied to either group. An additional issue is that saturation transfer is only one of many possible magnetic label-transfer approaches [see below, (36)] and that the "CEST" nomenclature for the agents is technically incorrect. Here we propose a classification based on the exchange mechanism (Fig. 3), namely atom (proton) exchange, molecular exchange, and compartmental exchange. This is valid for multiple nuclei [e.g., including Xe in hyperCEST (37)], but we will use proton terminology as this dominates the field (>99%). The proton transfer enhancements (PTE) attainable for these classes can be found from the product of the number of contributing exchangeable protons (N_E) per contrast agent (CA), the exchange rate that determines the effect (slowest if there are more than one), and

Table 1
Approximate Ranges for Exchange Rate, Proton Transfer Efficiency (PTE, Eq. 5) and Proton Transfer Ratio (PTR, Eq. 9) of Selected CEST Contrast Agents at Specified Solute Concentrations

	k_{sw}-range (s^{-1})	Functional group	Molecular unit	N_E	PTE/100[a]	[solute] μM	PTR (%)[a]
Proton exchange	10–30[b]	NH (APT)	Multiple unknown amino acids	5.5[c]	0.348–1.04	72,000	2.25–6.75
	20–1200[d]	NH	L-Lysine	7.8[e]	0.988–14.8	100	0.01–0.65[e]
	500–10,000[f]	NH_2	L-Arginine	23.0[e]	72.7–1453	100	0.65–13.1[e]
	500–10,000[f]	OH	Glucose	33.3[e]	105–2107	100	0.95–18.9[e]
	2000–8000[g]	Imino proton	Polyuridylic acid	3.1[e]	3.93–58.9	100	0.04–0.53[e]
Molecular exchange	2000–10,000[h,i]	Bound water	Eu-DOTA-4AmCE	4.0[j]	50.6–12,642	100	0.45–2.27[j]
Compartmental exchange	10–250[k]	Liposomal water	H_2O in 100 nm liposome; R(inner) = 95 nm[k]	240,000[l]	15,147–378,665	0.25	0.34–8.51[l]

[a]For $\alpha = 1$, $T_{1w} = 1$ s, $t_{sat} = 1$ s.
[b]Ref. 25.
[c]Average effect based on in vivo effect size for composite resonance at 3.5 ppm from water (23,25).
[l]Ref. 18.
[e]Per kDa (Eq. 6)
[f]Ref. 39.
[g]Ref. 24.
[h]Maximum rate is really 500,000, but only up to 10,000 included here because of saturation efficiency limits.
[i]Ref. 40.
[j]Per kDa (Eq. 7).
[k]Ref. 38.
[l]Per compartment (Eq. 8).

the attainable saturation efficiency at a power level reasonable for in vivo human and animal experiments. Thus, one has

$$\mathrm{PTE} = N_E \cdot \alpha \cdot k_{sw} \cdot T_{1w}\left(1 - e^{-t_{sat}/T_{1w}}\right), \quad [5]$$

in which

$$N_E = N_{CA} \cdot M_{CA} \quad \text{for proton exchange,} \quad [6]$$

$$N_E = C_m \cdot N_m \cdot M_{CA} \quad \text{for molecular exchange,} \quad [7]$$

$$N_E = 2 \cdot N_A \cdot [H_2O] \cdot V_{comp} \quad \text{for compartmental exchange.} \quad [8]$$

N_{CA} is the number of exchangeable nuclei (generally protons) per kiloDalton (kDa), M_{CA} the molecular weight in kDa of the contrast agent, C_m is the number of molecules coordinated per kDa, and N_m the number of protons in the coordinated molecule; N_A is Avogadro's number (6.0×10^{23} molecules $mole^{-1}$), $[H_2O]$ the water concentration (55.6 M) and V_{comp} the compartmental volume in liters. For a spherical liposome with internal radius R, V_{comp} would be $4\pi R^3/3$. The exchange rate for a liposome depends on the permeability, size, and membrane constituents of the particle (6,7,38). With respect to the classification, it may at first seem as if proton and molecular exchange are the same. But this is not true. In proton exchange, the protons are labeled and the individual exchange rate of the protons determines the PTE. For molecular exchange, contrast depends first on the lifetime of the coordinating molecule on the agent and subsequently on the exchange rate of the proton on the coordinated molecule. If the coordinated molecule is water, this cannot be distinguished from proton exchange, but it can be if it is any other molecule (e.g., a bound alcohol) containing its own exchangeable protons. In that case, the slowest of the two exchange steps towards water protons needs to be used for k_{sw} in Eq. 5, while the rate for the faster step determines the labeling efficiency in Eq. 4. The recent hyperCEST approach (37), employing exchange between nonlabeled and hyperpolarized Xe molecules can fall in either of the classes and a XTE (Xenon Transfer enhancement) can be calculated. For this review we focus only on protons.

Each of the three classes has distinctive advantages and disadvantages. Efficiency seems to depend predominantly on the exchange rate and the number of exchangeable protons per molecule or particle, but this can be misleading. With respect to the exchange rate, it should clear from Eq. 4 that an increased exchange rate will reduce saturation efficiency unless high B_1 can be used, which may not be the case in humans due to SAR restrictions and amplifier duty cycle limitations. In general, it is fair to say that for a contemporary high-end clinical field strength of 3 T, RF irradiation for a period of a second will be limited to powers less than 10–20 μT for the head coil and about 2–3 μT for the body coil. At 7 T these limitations will be more severe because the power deposition increases with the square of the field strength. In Fig. 4a, we evaluate α for the range of exchange rates covering all contrast mechanisms and a power range from 0.1 to 10 μT. It can be seen that the molecular exchange agents as well as rapidly exchanging OH, imino and amino groups for proton exchange compounds (Table 1) have low saturation efficiencies, while amide protons and compartmental exchange particles seem to be in the perfect k_{sw} range of 10–250 Hz. A more balanced view of the competition between saturation efficiency and the exchange rate can be obtained by plotting

the product $\alpha \cdot k_{sw}$ (Fig. 4b) versus k_{sw}, showing very acceptable performance of the high-rate compounds at 2 μT and already an order of magnitude higher effect at the still reasonable power level of 5 μT. Thus, it should be possible to study some of the slower exchanging paraCEST agents in humans. In addition, future developments in chemistry may allow reductions in the exchange rate (5,41). The parameter N_E should be optimized in terms of the number of exchangeable protons per molecule or compartment (denoted "solute" for convenience), because this will lower the concentration needed to see a measurable effect. For pure exchange, the PTE is related to the measured signal change and the PTR through:

$$1 - S_{sat}(\Delta\omega)/S_0 = \mathrm{PTR} = \frac{[\mathrm{solute}] \cdot \mathrm{PTE}}{2[H_2O]}. \quad [9]$$

One type of comparison between different agents can be made by calculating the solute concentration needed to achieve a 5% effect under typical in vivo conditions in humans. This is shown in Table 1 and plotted on a log scale in Fig. 4c. It can be seen that lipoCEST has by far the best return per unit and requires little power. APT requires little power and has the benefit of a high concentration of total amide protons, allowing detection in vivo in animals and humans. For the other compounds, higher power is needed, but all of them can be detected at concentrations that should be achievable in vivo. Again, Fig. 4 and Table 1 should be seen as providing only rough guidelines as it is difficult to compare the different groups directly, because there is no normalization to the same solute volume. Also, different compounds vary in toxicity and some may allow only very low concentrations. So each approach and solute has to be evaluated on an individual basis. Toxicity studies will have to point out which ones will be most suitable as contrast agents, with natural compounds such as sugars and proteins probably having the edge in humans. On the other hand, paramagnetic agents may allow the detection of smaller and/or more specific effects in animal models, leading to new discoveries.

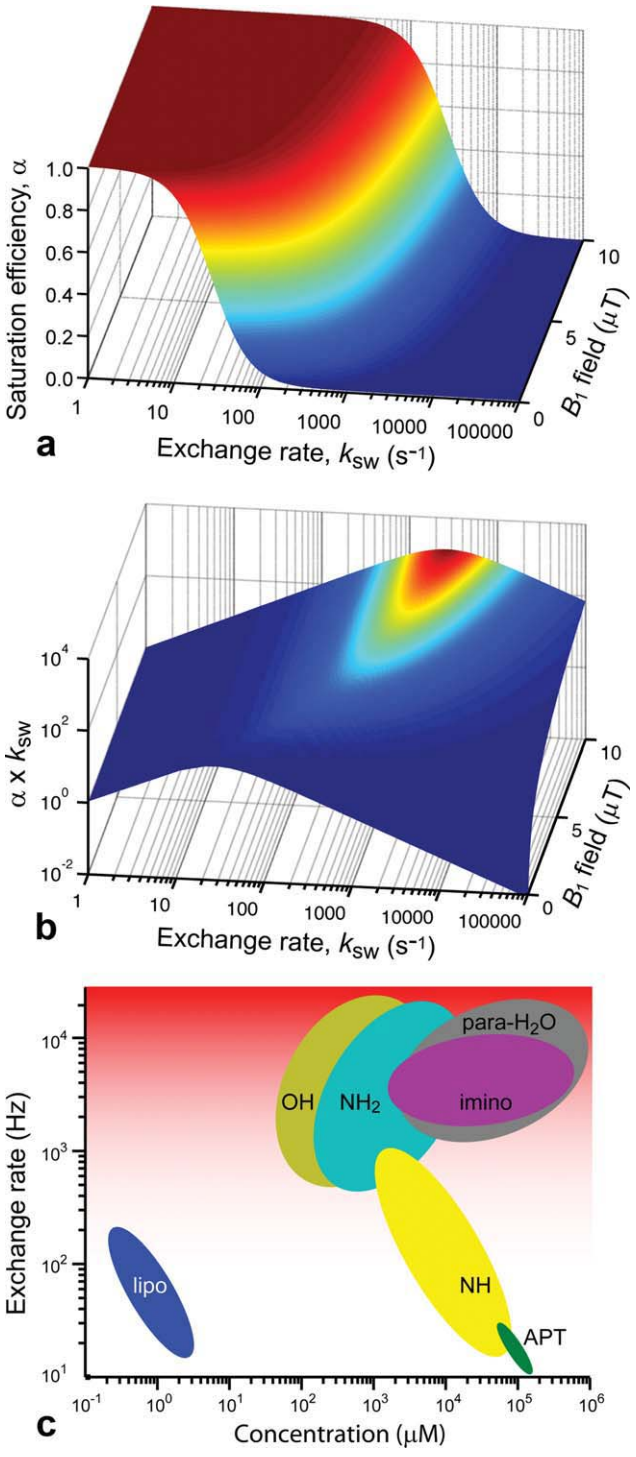

FIG. 4. Factors affecting detectability for the main classes of CEST agents. **a:** Effects of exchange rate (log plot) and RF field B_1 on the saturation efficiency (Eq. 4) for the B_1 range typically used on clinical scanners for SAR-compatible saturation experiments. Saturation transfer efficiency reduces with increased exchange rate, which can only be overcome by increasing B_1. **b:** Dependence of the product of saturation transfer efficiency and exchange rate on k_{sw} and B_1, showing that the increase in rate sufficiently compensates for the lost efficiency at clinically reasonable power levels. **c:** Log-plot of concentrations needed to achieve a 5% CEST effect for the different groups of agents. Notice that the curves for proton exchange and molecular exchange agents are affected by molecular size, while the compartmental exchange curve depends on particle radius, affecting both exchange rate and number of protons. Also, it is important to realize that paraCEST agents can be found in all three classes and water is normally the solvent, which is why we used para-H_2O to indicate molecular exchange. Graph is only approximate and meant to provide rough guideline. [Color figure can be viewed in the online issue, which is available at wileyonlinelibrary.com.]

Exchange and Cross-Relaxation in Liquids and Semisolids

The previous sections discussed the pure CEST mechanism (what's in the name). However, exchange is only one of several possible types of MT pathways that may contribute to saturation transfer experiments. It is well known from basic NMR (42–44) that chemical exchange and dipolar cross-relaxation pathways are active together in most MT experiments and difficult to separate completely. The relative contributions of these pathways may

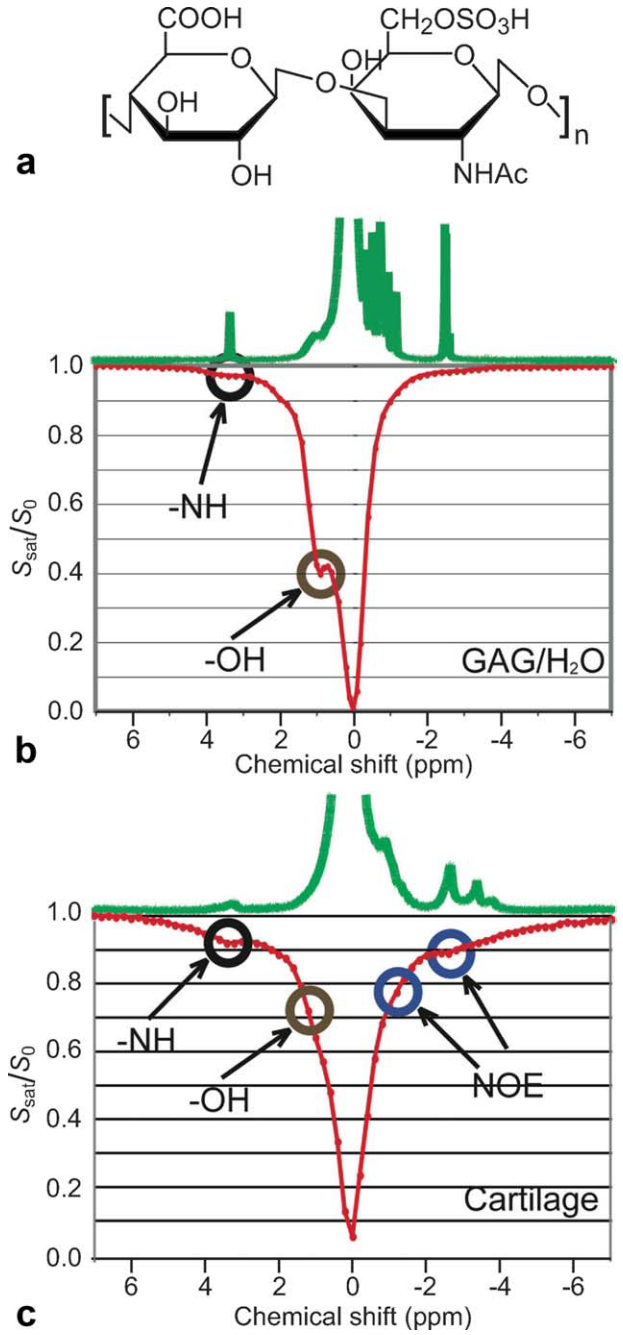

FIG. 5. Z-spectra for glycosaminoglycans (gags) in solution and in cartilage showing CEST and cross-relaxation effects (PBS, 11.7 T, t_{sat} = 4 s, 2.35 μT, 37°C). **a:** structure of gag-unit, showing three OH groups, an amide proton and several aliphatic protons in the ring (CH) and the *N*-Acetyl side chain. **b:** Z-spectra of 125 mM gag units in solution, showing predominantly NH and OH exchange saturation transfer effects. **c:** Z-spectra of cartilage from bovine patella in PBS buffer showing exchange and much increased cross-relaxation [nuclear Overhauser enhancement (NOE)] effects. Reproduced with permission from Ling et al., Proc Natl Acad Sci USA 2008;105:2266–2270. [Color figure can be viewed in the online issue, which is available at wileyonlinelibrary.com.]

vary with the type of excitation scheme used and depend on the molecular mobility and conformation, which will affect dipolar transfer efficiency and water accessibility, respectively. A beautiful example of the simultaneous occurrence of these effects is present in the work by Ling et al. (34,45), who studied glycosaminoglycan (gag) molecular units (Fig. 5a) in solution and in tissue. In solution, the exchangeable OH and NH groups show clear CEST effects at the hydroxyl and amide proton frequencies (Fig. 5b), while only a small saturation effect is visible upfield (i.e., at lower frequency) from water. In tissue, this upfield effect increases dramatically, even showing somewhat distinct effects at −1.0 and −2.6 ppm, corresponding to the CH and *N*-acetyl residues in gag. The origin of these effects was somewhat uncertain and the occurrence of nuclear Overhauser enhancement (NOE) effects, a type of cross-relaxation, between the side groups and water was suggested as a possible source.

The discovery of upfield saturation phenomena is important, both as a possible new source of MRI contrast as well as a possible nuisance with respect to performing the MTR asymmetry analysis used commonly in CEST experiments (Fig. 1, Eq. 1). To get a better understanding of the competing MT processes in medium sized macromolecules, it is possible to study the inverse effect through direct magnetic labeling of water molecules using saturation or inversion and to measure the effect on the proton spectrum as a function of time. This so-called Water-EXchange filter (WEX) experiment has been done for macromolecules in solution (46–48) as well as on perfused cancer cells and in vivo in the brain (49,50). Figure 6a shows the transfer mechanisms that are active after inversion labeling of water. In addition to direct proton exchange, there are exchange-relayed intramolecular NOEs, in which inversion is transferred from water to the molecule through rapidly exchangeable groups (mainly OH and NH_2, but also NH) and subsequently to the backbone aliphatic protons. In this particular experiment, a second cross-relaxation effect (direct intramolecular NOE) occurs because of simultaneous inversion of the C(α)-H protons that resonate close to the water frequency. The exchange-relayed NOEs and intramolecular NOEs build up slower than the proton exchange, which is illustrated for perfused cancer cells in Fig. 6b, where the NH proton intensities at 8.3 ppm (corresponding to about +3.5 ppm in a CEST spectrum) increase rapidly with time, followed by a slower rise of the aliphatic signals. The sign of the NOE effects is the same as for the exchange effects (in-phase), which is typical for intramolecular NOE effects in larger macromolecules in the slow rotational correlation time limit of the extreme narrowing regime. A similar effect can be demonstrated in brain (Fig. 6c), reflecting the presence of mobile macromolecules for which the proton transverse relaxation times are sufficiently long to allow observation in the NMR spectrum. In MTC and CEST experiments, where saturation is transferred to water, the opposite processes are involved. For mobile macromolecules this would lead to exchange-relayed transfer of saturation from the aliphatic protons to water. Notice that, in principle, intermolecular NOEs between bound water molecules and the solutes could also occur, but, for mobile macromolecules, these generally occur on a time scale much slower than exchange-relayed NOEs (46,51). For MTC studies, on the contrary, the motional limit is sufficiently slow for efficient intermolecular NOE transfer with bound water,

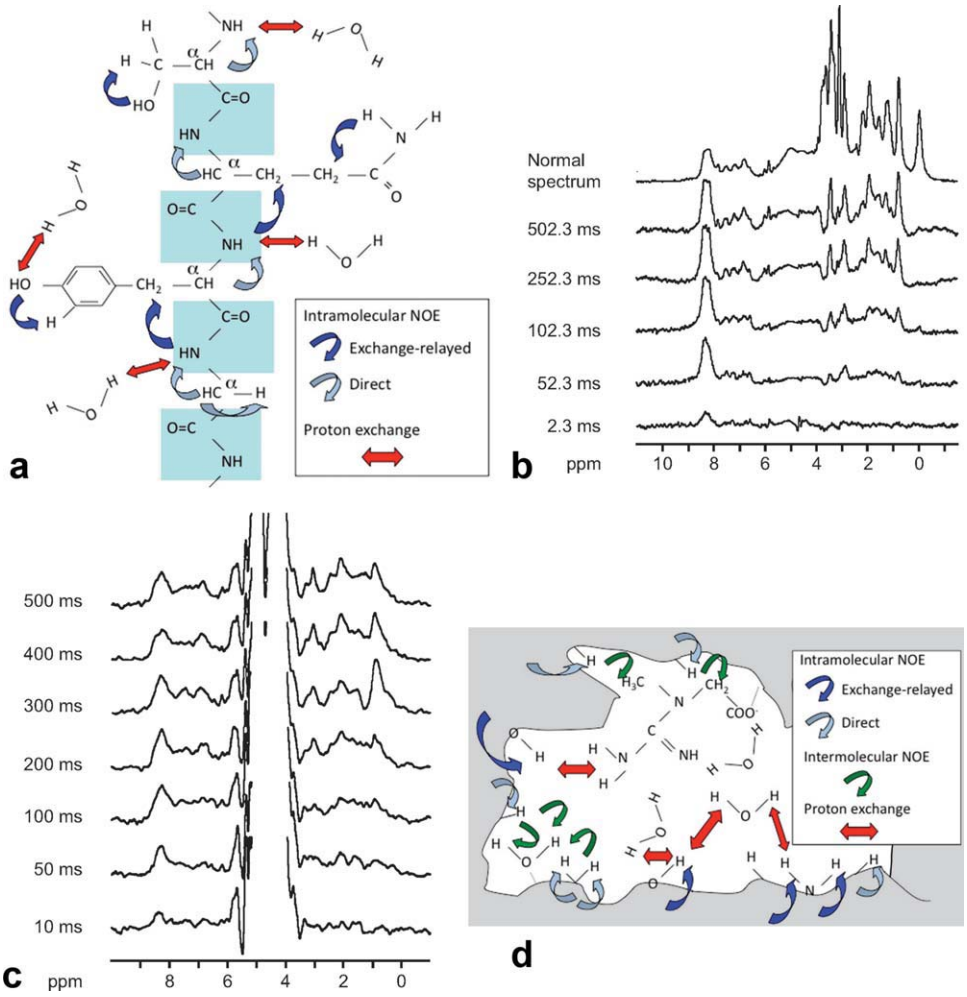

FIG. 6. Illustration of magnetization transfer pathways in proteins. **a:** Possible pathways in a mobile protein during a water exchange (WEX) experiment consisting of selective magnetic labeling (inversion) of bulk water (inverse of CEST/MT approaches) followed by a waiting period. Chemical exchange (red) and cross relaxation (blue) occur, the latter either exchange-relayed or through direct excitation of C(α) protons. These pathways are seen in cancer cells (**b**) as well as rat brain (**c**), showing fast buildup of exchangeable proton signals (especially amide protons at 8.25 ppm) as a function of time after inversion followed by gradual transfer to aliphatic protons through intramolecular NOEs. **d:** Transfer processes occurring during an MTC experiment. The semisolid matrix, where fast intramolecular dipolar transfer occurs, is indicated in grey. Contrary to mobile proteins, the effects of both exchange and intermolecular NOEs with bound water can be substantial. Reproduced with permission from van Zijl et al., Magn Reson Med 2003;49:440–449. [Color figure can be viewed in the online issue, which is available at wileyonlinelibrary.com.]

which occurs together with exchange-relayed transfer (Fig. 6d). Here, the exact proportions of these contributions are still under debate. Within the semisolid lattice itself, all saturation is efficiently transferred through spin diffusion (fast through-space dipolar transfer), which can subsequently be transferred to water though the mentioned processes.

In the presence of multiple molecular systems, such as in cells and tissue, all of the above phenomena take place, complicating the data interpretation. In addition, the simultaneous occurrence of multiple transfer effects invalidates the two-compartment assumption for CEST quantification. In Fig. 7a, the in vivo Z-spectra of several brain regions are shown for a rat with an implanted brain tumor. For the multipulse sequence used there are large MTC effects on which the smaller CEST effects should be superimposed. When trying to extract the CEST effects using MTR asymmetry analysis (Fig. 7b), a clear residual asymmetry is found that has been attributed to MTC effects that are not centered around the water frequency (52–54). Fortunately, most of this MTC asymmetry can be removed through comparison with normal tissue (Fig. 7c), which is assumed to display only the inherent asymmetry reflecting the CEST PTR. Interestingly, this remaining PTR difference shows several percent increase for the tumor while a negligible change is found for edematous areas, indicating the possible separation of these two regions for clinical application. Similar competition between MTC and CEST effects can be seen in a rat model of cerebral ischemia (Figs. 7d–f). Contrary to brain tumors though, a comparison with normal tissue shows a reduction in PTR.

Based on the likely origin of this effect in the exchangeable amide protons of mobile tissue proteins and peptides ((25,49,50), Fig. 6c), this contrast was dubbed Amide Proton Transfer (APT) MRI. In addition

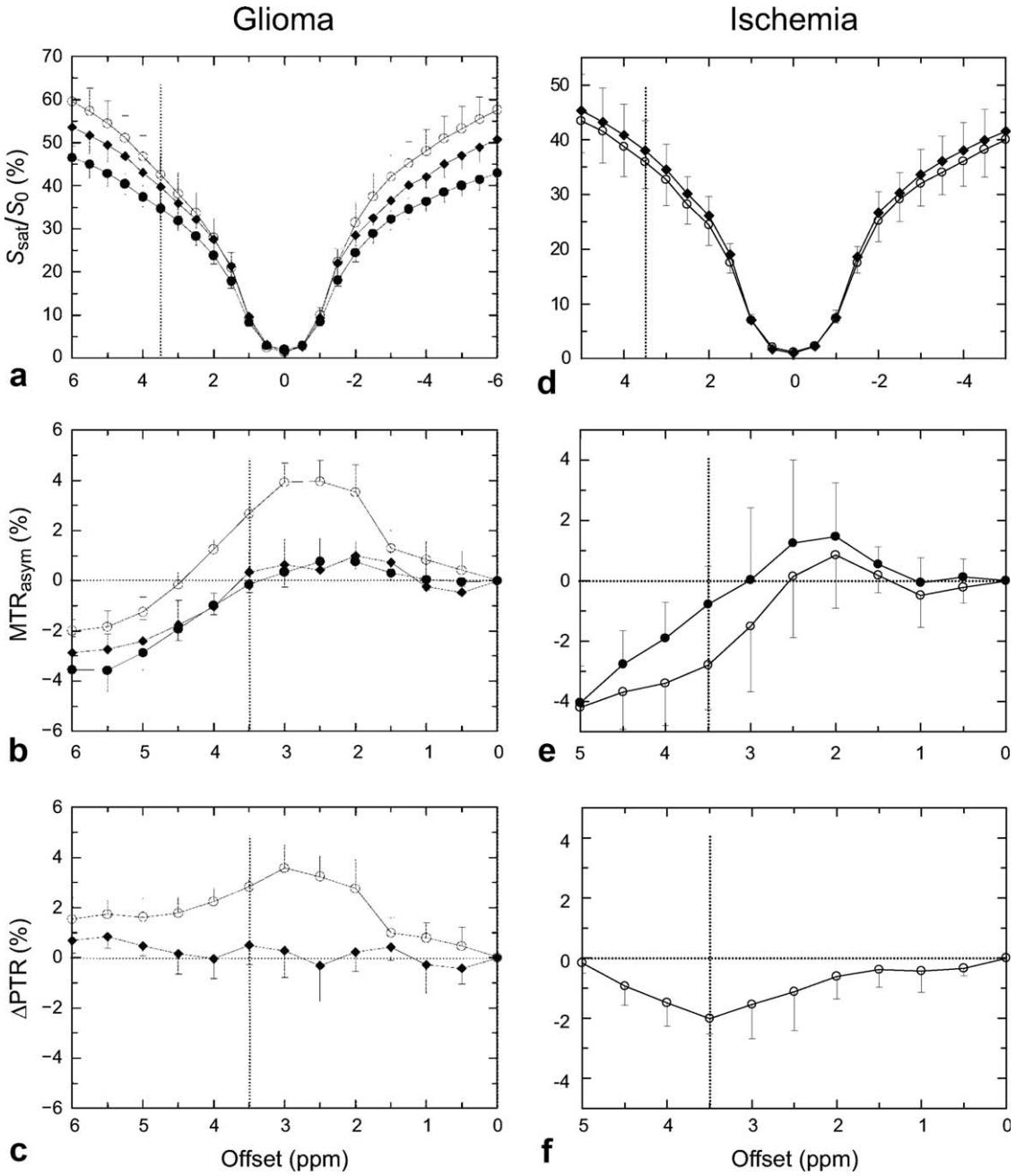

FIG. 7. Effect of MTC on Z-spectra and CEST data analysis for 9L glioma (**a–c**) and ischemia (**d–f**) in rat brain (Multipulse saturation: 400 gaussian 180° pulses, 4.7 T, $t_{sat} = 4$ s, $B_1 = 1.2$ μT). Solid circle: contralateral brain; diamond: peritumoral tissue (a–c); open circle: tumor (a–c) or ischemic lesion (d–f). Signal attenuation in Z-spectra (a, d) is due mainly to direct water saturation close to the water frequency and a large MTC effect (40 to 60%) over the whole spectral range. The MTC contribution is reduced for edema and tumor (a), indicating a higher water content for these tissues. The Z-spectra are slightly asymmetric, which becomes visible when performing asymmetry analysis (b, e). Both exchange effects and asymmetry in the MTC contribute to the residual curve, with the latter reflected in a relatively constant negative MTR_{asym} (2–3%) at offsets above 5 ppm. The PTR for tissue changes can be estimated by comparing lesion with normal brain, removing most of the MTC effects (c, f). This shows that edematous regions can be separated from tumor (c) and ischemia from normal brain (f). The positive (c) and negative (f) PTR differences were attributed to increases in protein content and reduced pH, respectively. Reproduced with permission from Zhou et al., Magn Reson Med 2003;50:1120–1126 (a–c) and Nat Med 2003;9:1085–1090 (d–f).

to the maximum APT effect at around 3.5 ppm from water, it seems likely that multiple exchangeable groups contribute as the effect ranges over offsets from about 1–6 ppm from water. The APT in tumors is positive (Fig. 7c), while an opposite effect is found in acute ischemia (Fig. 7f). The explanation for the difference follows from the contributions in Eq. 2. During acute ischemia brain pH reduces, thereby reducing the amide proton exchange rate (44,55), while amide proton content remains approximately constant, which could be shown with WEX

spectroscopy (25). The tumor, on the other hand, has increased cellular amide proton content (see Fig. 6b as illustrative example for another tumor type) compared to normal brain, while intracellular pH (not extracellular) is known to remain approximately constant (56,57). In the acute ischemia study (25), ΔPTR was also calculated over a range from 0 to 15 ppm from water by comparing ischemic brain with normal. The result showed removal of the asymmetry in MTC, leaving only a negative effect over the range from about 1–6 ppm downfield from water, in line with the expected exchangeable amide proton range in the NMR spectrum.

In summary, saturation transfer studies in vivo are affected by exchange, exchange-relayed NOEs, and intermolecular NOEs (semisolid components). Depending on the materials studied or the pulse sequence parameters used, the relative contributions of each of these mechanisms may vary. For instance, paraCEST agents and other compounds with very rapidly exchanging protons will predominantly show CEST-based MTR asymmetries, while macromolecular proton exchange species may show NOE effects. Increasing the power of the saturation field will increase the MTC contribution, which may negate the slower mobile protein NOE effects and vice versa. This sensitivity to multiple mechanisms and to pulse sequence parameters complicates comparison of MTC and CEST studies between laboratories. It has been a bottleneck for clinical trials studying the use of MTC as a biomarker and will no doubt affect such efforts for CEST studies. However, this multifaceted character also opens up opportunities to assess different cellular components and different transfer processes by varying MRI parameters, which is the topic of the next section.

Pulse Sequences for Studying Exchange Effects

CEST labeling is very similar to MTC labeling in that a pulse sequence is applied to measure the presence of a small pool indirectly via the solvent, which can be done by saturating the small pool and allowing magnetization to transfer between the pools. For MTC, this has led to a range of approaches [for some reviews, (58–64)] employing both on-resonance and off-resonance saturation. In the classical continuous saturation, long (several seconds) low power off-resonance RF irradiation is used with the goal of equilibrating the populations of the two quantum states of the semisolid protons. While doing so, partial saturation is transferred continuously to bulk water. Alternatively, one can apply a series of frequency-selective off-resonance pulses for saturation using higher-power pulses of medium length (millisecond to tens of milliseconds) spaced by ms-length time intervals. This is repeated continuously to build up and maintain a saturation steady state (62–67), which can be done in a multistep preparation as well as in single steps between different k-space acquisitions, for instance when using 3D imaging. The most sensitive approach to reduce the water signal through MT is using multistep on-resonance "saturation" (64). The quotation marks are added to stress that this is not saturation in the classical sense of population equilibration, but rather randomization of magnetization through dephasing. In these experiments the bulk water pool is quickly excited and returned to equilibrium, thereby not really affecting free water, which has a long T_2^*. The semisolid pool, however, has a T_2^* (and T_2) on the order of microseconds and rapidly loses coherence due to random dephasing. As a consequence, longitudinal coherence is lost after each excitation flip-back step. Notice the inherent beauty of this powerful scheme is that it has high "saturation" efficiency for the immobile macromolecules since all excited spins are dephased within microseconds. It should be noted that the pulsed off-resonance scheme is a hybrid approach as it has both classical saturation and dephasing contributions. A third type of MTC scheme (68) is to monitor the recovery of the bulk water pool after a nonselective single inversion pulse, which shows bi-exponential behavior due to the interaction with the semisolid pool.

Intuition indicates that CEST effects should be detectable in a manner similar to MTC, and most CEST studies have employed either continuous (Fig. 8a) or pulsed (25,33,69,70) selective off-resonance saturation of the exchangeable protons. Recently, Vinogradov et al. (71,72) have shown that the presence of micromolar concentrations of paraCEST a gents can be detected using an on-resonance pulse scheme in which water signal is continuously undergoing 360° rotations in a WALTZ multipulse scheme compensated for B_1-inhomogeneity. Notice that this on-resonance paramagnetic exchange effects (OPARACHEE) approach differs from the on-resonance MTC schemes in that the small pool is not excited and that, therefore, its frequency does not need to be known. After a series of such pulses, water signal is reduced due to magnetization exchanging from bulk water to the contrast agent, leading to part of the magnetization not experiencing full 360° pulses. This technique, employing a low-power RF train, is suitable for detecting rapidly exchanging units, such as the water molecules in molecular exchange agents and OH and NH_2 groups in proton exchange agents (if their excitation can be avoided). Similar to standard CEST, however, DS of water reduces the sensitivity and complicates quantification. A disadvantage of OPARACHEE is that it cannot distinguish between different agents or chemically different protons, but it may be the most suitable approach for detecting single agents.

Another interesting phenomenon reported recently is that MT effects are enhanced (73) when using intermolecular multiple quantum [iMQC, (74)] excitation schemes. The double quantum (DQ) analogue of this was recently demonstrated for CEST MRI (45,75). Unfortunately, even after enhancement, the iDQC signal to noise ratio (SNR) is still only about 25% of the standard CEST effect, which reduces its applicability in the clinic (75).

When thinking about alternative CEST technology, it is fundamental to realize that saturation is just one type of magnetic labeling and that many other approaches have not yet been explored. Importantly, CEST compounds differ from the semisolid MTC protons in transverse relaxation properties ($T_{2\text{mobile}}^* \gg T_{2\text{solid}}^*$) and average exchange rate [$k_{\text{CEST}} \gg \langle k_{\text{solid}} \rangle$, which is only 4–8 Hz in the brain (76–78)], which opens up a new range of labeling approaches that cannot be applied to MTC. Such methods may inherently provide new opportunities

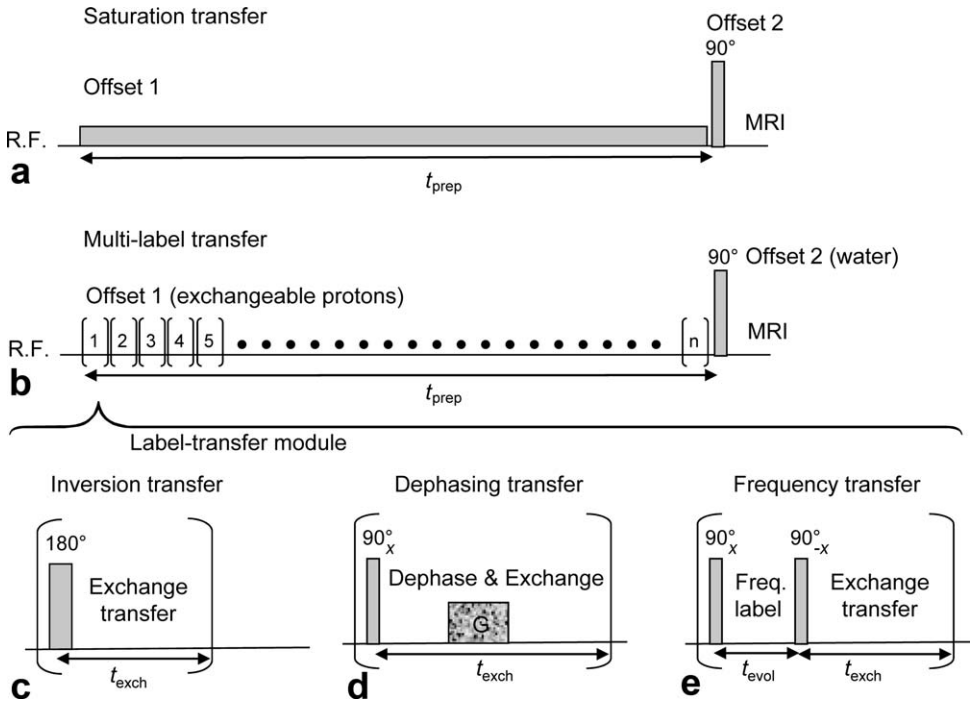

FIG. 8. Possible schemes for exchange transfer MRI. **a:** Standard CEST: protons are labeled through continuous saturation and transferred continuously during labeling. **b:** Exchange transfer using label-transfer modules (LTMs): protons are rapidly labeled through either selective inversion (**c**) or selective excitation followed by a magnetic manipulation (**d, e**). This can be gradient dephasing (**d**) or frequency labeling during an evolution time t_{evol} followed by selective flipback to the *z*-axis (e). After labeling, exchange transfer to water protons occurs during t_{exch}. The label transfer modules, (*n* total), are repeated continuously during preparation period t_{prep} to enhance the effect on bulk water. The water labeling efficiency depends on the exchange rate, which, together with the power deposition limits, determines the number of modules that can be used.

for separating MTC and CEST effects. At first it seems impossible to enhance sensitivity without the continuous saturation labeling that is at the foundation of CEST imaging and even imbedded in its nomenclature. However, building up saturation is actually quite inefficient compared to RF excitation, which can label spins almost instantaneously. Of course, this label exchanges to water, and the process has to be repeated for excitation processes to be able to accomplish enhancements similar to continuous saturation. Recently (36), it was shown that this can be achieved by using a series of so-called label-transfer modules (LTMs), in which exchangeable solute protons are selectively labeled, and subsequently transferred to water (Fig. 8b). Signal amplification occurs because fresh *z*-magnetization is present for the solute protons at the start of each LTM, allowing serial transfer of labeled protons to water when applying multiple (*n*) modules during the preparation time, t_{prep}. This novel principle allows several labeling types to be used, including inversion (Fig. 8c), dephasing (Fig. 8d) and frequency encoding (Fig. 8e). The first two are "saturation-like" approaches in that they reduce the water signal intensity. In the inversion approach, the *z*-magnetization transferred is of sign opposite to the equilibrium water magnetization, and, as such, twice as efficient as continuous saturation, where zero longitudinal magnetization is transferred. The dephasing approach differs from the MTC dephasing approach (employing the short T_2^* of solids) in that protons of interest are excited selectively and that dephasing of transverse magnetization need not be relaxation-based, but can be induced coherently by a pulsed gradient. For very rapid exchange, the dephasing gradient may not be needed as all spins will be transferred to water quickly where they dephase slowly with T_{2w}^*. Frequency labeling (Fig. 8e) has never been used for MTC. It has the potential to extend in vivo MT measurements with high-resolution NMR type multidimensional experiments and high-resolution experiments with the advantage of exchange based sensitivity enhancement through the water signal. The principles of this approach, dubbed frequency-labeled exchange transfer [FLEX, (36)], are explained in Fig. 9 using the example of a mixture of protons of different concentrations and exchange rates.

To get a first impression of the contributions to LTM-based exchange transfer, appropriate two-pool equations can be derived under the assumptions that (i) the length of the labeling module is much shorter than T_1s of water and the exchangeable protons, (ii) the exchange rate is much faster than $1/T_1$ of the exchangeable protons, (iii) there is negligible back exchange from water to agent protons (36):

$$\mathrm{PTR} = x_s \cdot \lambda \cdot A \cdot \left(1 - e^{-k_{sw} \cdot t_{exch}}\right) \cdot \sum_{i=1}^{n} e^{\{-1+(i-1)/n\} t_{prep}/T_{1w}}. \quad [10]$$

Similar to the CEST theory (Eqs. 2 and 3), the expression contains terms for proton fraction, labeling efficiency ($\lambda \cdot A$), exchange transfer efficiency ($1 - e^{-k_{sw} \cdot t_{exch}}$), and water relaxation. The parameter λ describes the LTM excitation efficiency, while $A = 2$ for inversion and $A = 1$ for the

dephasing and FLEX approaches. Notice that exchange transfer efficiency will depend on k_{sw} for inversion and FLEX experiments, but not for dephasing, where the exchange time (t_{exch}) equals t_{prep} for the first LTM and becomes shorter as a function of LTM number. This efficiency term provides capability for exchange filtering. For instance, for rapidly exchanging protons (e.g., $k_{sw} > 2000\ s^{-1}$) one would have 86% efficiency of transfer when using exchange time of 1 ms and 98% for 2 ms. For slower protons (e.g., $k_{sw} \approx 20\ s^{-1}$), these efficiencies would be 2.0% and 3.9%, respectively, and t_{exch} has to be made longer. The summation term reflects that magnetization transferred in the first LTM will experience T_{1w} decay over the full t_{prep}, while that transferred in the nth module will hardly relax.

While CEST, inversion transfer, and dephasing transfer all lead to a signal decrease in the water signal, FLEX detection is different in that the water signal is modulated as a function of evolution time [Fig. 9c, (36)] in a manner depending on the frequency difference between the offset (o1) of the 90_x excitation pulse and the solute resonances ($\Delta\omega_{so1}$). This can be described by a free induction decay (FID):

$$I_{w,tot} = \sum_s PTR_s \cdot e^{-\left(k_{sw}+1/T_{2s}^*\right)\cdot t_{evol}} \cdot \cos(\Delta\omega_{sol} \cdot t_{evol}). \quad [11]$$

Notice that the exponential signal decay term provides the opportunity to remove rapidly decaying components, such as semisolids (short T_2^*), or select different components based on exchange rate. The FLEX approach illustrates the power and beauty of MR where the transfer effect of multiple magnetic species, even though detected through one species (water protons) can still be separated out (Fig. 9). The complete arsenal of techniques for FID analysis is applicable (42,43), including deconvolution techniques such as exponential line-broadening, Lorentzian-Gaussian deconvolution, deconvolution-difference to remove broad components, and especially time domain analysis. The latter is extremely suitable because, when using contrast agents, the presence of only a limited number of components with known frequencies in the FID should allow straightforward interpretation.

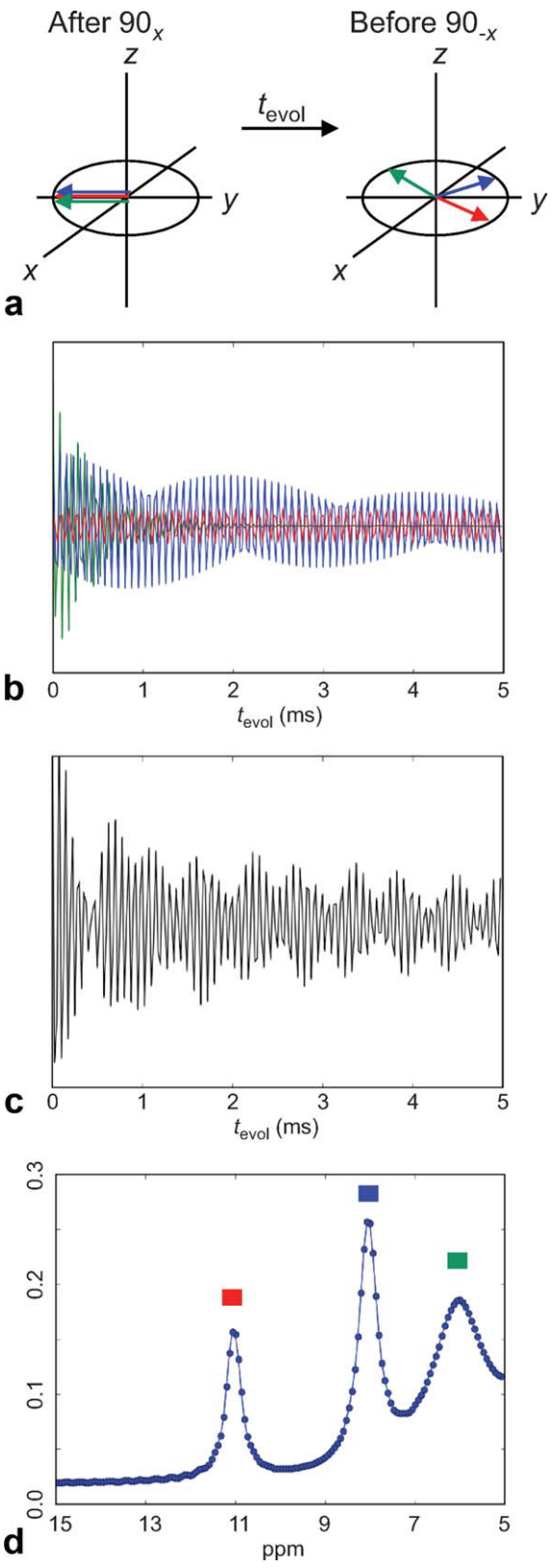

FIG. 9. Principle of frequency labeled exchange transfer (FLEX). A range of frequencies including multiple exchangeable protons is selectively excited (90_x pulse, Fig. 8e), after which chemical shift evolution separates the different frequency components (red, blue, green). Depending on t_{evol}, a different size of magnetization component is flipped back to the z-axis by the 90_{-x} pulse (**a**) and transferred to water protons. When performing a series of acquisitions at different evolution times, a free induction decay (FID) containing the multiple frequency components is obtained (**b**). These components are all part of a single water signal and nondistinguishable (**c**). However, Fourier transform of the convoluted decay can recover a frequency spectrum (**d**), allowing separation of the three different components based on frequency (chemical shift) and exchange rate (peak width). The normal ^{1}H NMR spectral frequencies were used with water assigned to 4.75 ppm. Parameters used in b–d: field of 14.1 T (600 MHz); offset frequency of RF pulse 25 ppm from water; dwell time 25 μs. Signals were green: 20 mM, 6 ppm, $k = 2000$ Hz; blue: 10 mM, 8 ppm, $k = 200$ Hz; red: 5 mM, 11 ppm, $k = 20$ Hz. FID processed using 20 Hz exponential line broadening and zero filling by a factor of four. Courtesy of Josh Friedman, Johns Hopkins University. [Color figure can be viewed in the online issue, which is available at wileyonlinelibrary.com.]

A disadvantage of pulsed approaches is the danger of high power deposition, but this can be avoided by using a sufficiently low average power over the total scan repetition time (TR), which can easily be optimized for each type of coil used. Similar to CEST, inversion and dephasing transfer may require acquisition as a function of frequency and correction for asymmetry with respect to the water signal. FLEX, on the other hand, may be performed without asymmetry analysis, but, similarly to multidimensional experiments, the length of the scan time will depend on the number of points sampled for the FID. The latter can probably be optimized by using sparse sampling schemes in the time domain (79–81), which is the topic of future research.

Signal and Parameter Quantification

Proper quantification requires careful measurement of the CEST effects (uncontaminated and with sufficient SNR), which is far from trivial in view of the many contributions outlined in the previous sections. One universal requirement is to selectively label the protons of interest, which is complicated by "spillover" due to proximity in chemical shift of the solute and water protons for many diaCEST and lipoCEST agents or due to broadening of the DS contribution when using the higher B_1 fields needed for paramagnetic molecular exchange agents and rapidly exchanging proton exchange compounds. In vivo, the effects of MTC, contrast agent (CA) CEST and endogenous (endo) CEST compete and have to be separated out, which cannot be modeled by a two-pool compartment. The theories for three-pool and four-pool systems have been described (16,19,22), but most investigators tend to use a zero-order approach of additive effects:

$$\mathrm{MTR}^{\mathrm{total}} = \mathrm{PTR}^{\mathrm{CA}} + \mathrm{PTR}^{\mathrm{endo}} + \mathrm{MTR}^{\mathrm{MTC}} + \mathrm{DS}, \qquad [12a]$$

and

$$\mathrm{MTR}_{\mathrm{asym}} = \mathrm{PTR}^{\mathrm{CA}} + \mathrm{PTR}^{\mathrm{endo}} + \mathrm{MTR}^{\mathrm{MTC}}_{\mathrm{asym}}. \qquad [12b]$$

The reason that this is acceptable is that the multipool approaches require solving for multiple parameters, which may not improve accuracy due to the limited number of observables available and the already large number of MT contributions. Notice that Eqs. 12a and 12b neglect interference from NOE effects, which may have to be added in for certain agents as well as for the endogenous proteins. The FLEX method has a major advantage for quantification, because competing MTC and direct water excitation effects contribute differently to the time domain signal. The short-T_2^* components (Eq. 11) contribute only to the initial points during which they are incoherently dephased, while water modulation due to direct excitation occurs at a well-known offset frequency. As a consequence, both can be filtered out from the signals of interest (36) and the FLEX spectrum should be able to provide direct determination of PTR for the specific spectral lines without need for asymmetry analysis.

In CEST experiments, experimental determination of $\mathrm{MTR}_{\mathrm{asym}}$ is complicated by variation of the B_0 field over the sample or subject. Good asymmetry analysis requires exact knowledge of the water frequency in each voxel, which can generally be obtained by acquiring a full Z-spectrum and determining the center of the DS line shape. In clinical studies, however, this may be too time-consuming due to limited SNR and the concomitant need to acquire multiple scans. Therefore it has been suggested to acquire CEST data (multiple scans) for only a limited number of essential frequencies around $\pm\Delta\omega$, which is combined with the water frequency determined from a single Z-spectrum (82) or from a rapidly acquired gradient-echo-based field map (69). However, a Z-spectrum is still slow, while field maps are often complicated by the need for phase unwrapping, the presence of image distortions (especially at higher fields), and limited accuracy (several Hz) of the frequency differences. The latter is not an issue for shim optimization, but may be problematic for asymmetry determinations due to the steep shape of the DS contribution to the CEST spectrum. In an alternative referencing scheme, called WASSR [WAter Saturation Shift Referencing, (83)] a water frequency map is acquired using a saturation sequence with low B_1 and short t_{sat} (e.g., 0.5 μT, 50-100 ms), leading to a Z-spectrum dominated by DS (negligible interference from MTC and CEST). Because the shape of the DS line is symmetric (84) the water center frequency can be determined in each voxel with subhertz accuracy (83), of course depending on the field strength (WASSR-bandwidth) and number of points acquired. Similar to field mapping, the WASSR-scan can be acquired rapidly due to lower power deposition, and, if needed, with reduced spatial resolution (e.g., $4 \times 4 \times 4$ or even $8 \times 8 \times 8$ mm^3 in humans), and interpolated to high resolution for data processing. WASSR will be especially useful when there is overlap in the Z-spectrum between the CEST agent line shape and the saturated water signal shape, which causes an asymmetric broadening of the DS curve that prohibits accurate assessment of the exact water frequency.

Inhomogeneity in the B_1 field may also pose problems, because it leads to spatial variation in saturation efficiency. This will especially be a concern for solutes with fast exchange rates (Eq. 4), but not for endogenous APT, where complete spin saturation ($\alpha \approx 1$) is pretty much achieved for a B_1 range of 1–3 μT. For the LTM methods, the amount of signal may differ per voxel, but the signal modulation in FLEX should not. Inhomogeneity in B_1 is not expected to be a major issue in the near future in view of new multichannel transmit hardware becoming available for imaging (85,86).

A final issue complicating asymmetry analysis is the occurrence of image artifacts when studying amide protons. These protons have the same chemical shift difference with water (3.5 ppm) as lipid resonances but on opposite sides of water. When acquiring the amide saturation image, lipid signals are not suppressed. However, they are when saturation is applied at −3.5 ppm. In brain images, this can lead to dark rings close to the skull, especially when using phased-array coil reception for which skull lipid signals are picked up with very high SNR [Fig. 10, (87)]. To obtain an appropriate $\mathrm{MTR}_{\mathrm{asym}}$ image, the lipid signals should be suppressed equally when saturating at both offsets, which has been successfully demonstrated in multislice (88–90) and whole-brain

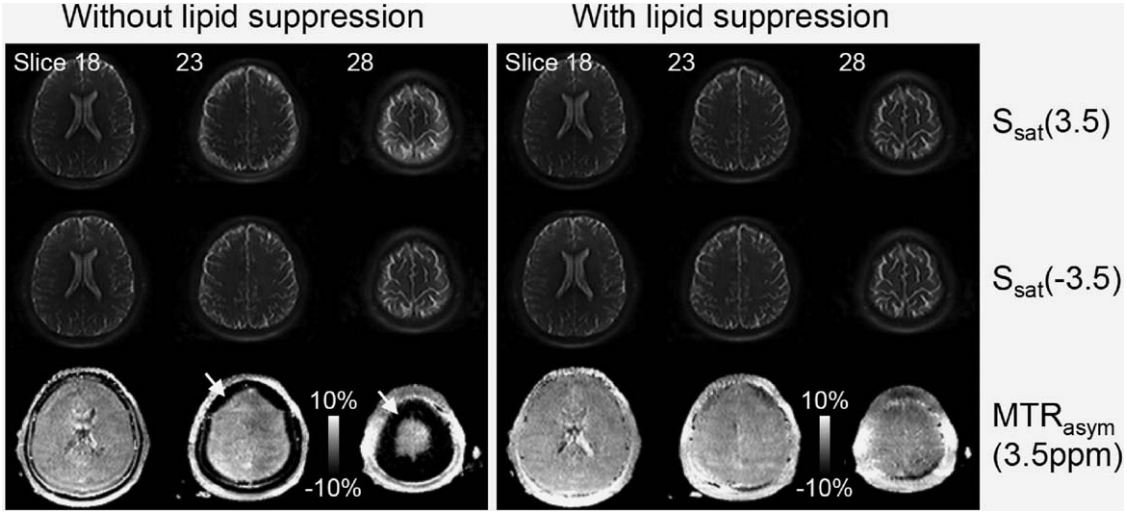

FIG. 10. Illustration of lipid interference and suppression in 3D amide proton transfer (APT) scanning in the human brain. 3D Gradient and spin echo (GRASE) acquisition with multipulse saturation preparation showing saturated images at ±3.5 ppm as well as the calculated MTR_{asym} (3.5 ppm) images for three slices (in three columns) without and with lipid suppression. Without lipid suppression, ring-like hypointensities (white arrows) appear in the MTR_{asym} (3.5 ppm) images, which are removed when applying a frequency-modulated selective lipid suppression pulse in both image acquisitions (±3.5 ppm). Reproduced with permission from Zhu et al., Magn Reson Med 2010;64:638–644.

3D APT imaging [Fig. 10, (87)]. When using EPI methods, ghosting artifacts from lipid signals in the scalp occur in the MTR_{asym} image, which can be removed similarly or through the use of frequency-selective refocusing pulses during spin echo acquisition (91).

Assuming that an appropriate PTR can be measured (uncontaminated and reproducible) the absolute quantification of a parameter requires availability of a theory to describe the effects (Bloch equations or its analytical solutions) and of the other parameters in the equations. For instance, when the solute concentration is to be determined, T_{1w} and k_{sw} need to be known and a concentration reference is needed. Measurement of T_{1w} can be done using conventional MRI techniques, while k_{sw} can be measured using either the WEX approach (Fig. 6) or through measurement of the CEST intensity as a function of saturation time or power (18,92). Exchange transfer measurements have the powerful property that water (111.2 M proton concentration) can be used as an internal reference standard (Eq. 9). Notice that this quantification in actual mM concentration units is possible because MRI measures the free water signal in which the agent is dissolved. If the concentration per voxel volume or per gram tissue would need to be known, a water density correction would have to be applied, but for most applications concentration in mM is what is needed. Using measured WEX exchange rates and APT intensities in the rat brain, it was possible to determine the in vivo amide proton concentration (8.3 ppm) to be about 72 mM (23,25), reflecting the total concentration for a large group of contributing proteins and peptides. The FLEX method seems very suitable for quantification, which was recently demonstrated for a DNA dimer in solution (Fig. 11) as a function of the number of LTMs used. The results show excellent correspondence of the experimental curves to Eq. 10 and gave a DNA concentration of 0.60–0.65 mM per duplex, comparing well to the experimentally estimated concentration based on nucleoside analysis (0.8 mM) and providing further validation of the FLEX method.

Depending on the type of exchangeable proton and the mechanism of exchange catalysis (base, acid or water catalyzed, buffer catalyzed), exchange rates may show pH dependence over a certain pH range. If this dependence can be calibrated under the appropriate in vivo conditions, e.g., using phosphorus spectroscopy as a reference (23,25), exchange transfer allows determination of absolute pH. A very elegant and more straightforward approach was suggested by Ward and Balaban (32), who used a ratiomeric approach for the PTR of two distinguishable protons with different pH dependence in the same molecule. This allows the effect of concentration to be removed according to:

$$\frac{PTR_1}{PTR_2} = \frac{N_{E1} \cdot \alpha_1 \cdot k_1}{N_{E2} \cdot \alpha_2 \cdot k_2}. \quad [13]$$

This principle may allow calibration in a buffered phantom and application in vivo, under the condition that the exchange mechanisms for the protons being compared would be negligibly affected between the conditions. Aime and coworkers (93,94) applied similar principles for assessing pH in a concentration-independent manner using paraCEST agents containing multiple groups in which the molecular exchange was pH independent and the exchange of amide protons contained in the complex pH dependent. Analogously, one could use two molecules with different protons (32), which was applied by Aime et al. for paraCEST agents (27). This latter approach of course requires the concentrations to be added back into Eq. 13, which may complicate in vivo application unless the relative concentration can be kept stable, which may be the case in a protected environment such as a liposome (6,95).

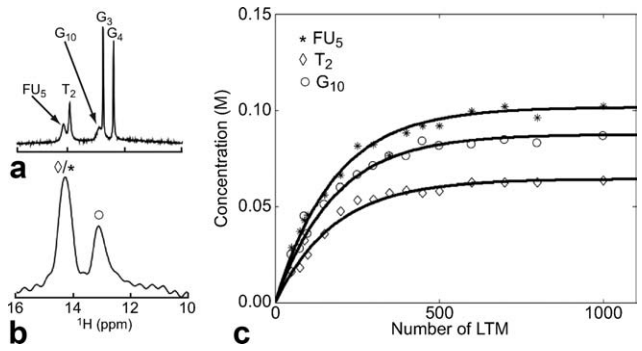

FIG. 11. Illustration of quantitative concentration determination using the FLEX method for the DNA duplex 5′-$C_1T_2G_3G_4FU_5A_6C_7$-$C_8A_9G_{10}$-3′ (T = 10°C; pH = 9.0; C = Cytosine; T = Thymidine; G = Guanosine; FU = Fluorouracil; A = Adenosine). **a:** Conventional jump-return spectrum in which all imino protons are observable. **b:** FLEX spectra in which G3 and G4 do not appear due to slow exchange. **c:** Absolute concentration of labeled protons generated by FLEX as a function of the number of applied LTMs. Data based on time domain fitting using prior knowledge of the chemical shift and decay rate. Black lines are best fits of data to Eq. 10 (concentration = PTR · 2 · [H_2O]). Reproduced with permission from Friedman et al., J Am Chem Soc 2010;132:1813–1815.

In Vivo CEST Imaging and Translation to Humans

CEST agents provide a powerful source for potential contrast (4,5,7,10,11), including pH imaging (18,25,27,32,56,70,93,94,96–103), metabolite detection (29,104–106), imaging of mobile proteins or peptides in tissue (25,33,82,107,108), metal ion detection (109,110), liposome labeling (6,7,35,111–114), nanoparticle/polymer labeling (31,101,115–117), protein-binding (118), RNA-protein binding (24), DNA-protein binding (119), temperature imaging (32,96,120–122), detecting enzyme activity (123–127), CEST reporter genes (128), and imaging of OH groups (26,34,99), polyamines (129,130), and nucleic acids (24). Similar to many other molecular imaging approaches, most CEST studies have been in vitro, and for a detailed overview of all contrast agent in vitro work to date, we refer the reader to several comprehensive recent reviews (3–5,9–11,131). Here we briefly discuss current progress in vivo and the potential translation to the clinic.

Clinical application requires the investigators to address several issues, including toxicity of the agents (when using exogenous contrast), limited scan time, the need to scan whole organs, and the danger of too much RF power deposition when performing MT experiments. Power deposition increases quadratically with field strength and transmit coil size. This restricts the use of certain MRI pulse sequences, as safety requires the average power over the scan repetition time (TR) to be within FDA-guided SAR requirements on human scanners. Staying within recommended SAR is not straightforward when using multislice or 3D acquisitions with continuous or pulsed saturation combined with band-selective lipid suppression pulses and spin echo acquisitions. This will be equally challenging for the repeated LTMs in the new exchange transfer approaches, which also employ series of high-B_1 pulses. However, history shows that a similar fear has not limited MTC studies, which smoothly moved from 1.5 to 3 T, even for whole organ studies. Recent support for this point of view comes from data showing the possibility to perform multislice (88,90) and 3D (87) CEST at 1.5 T, 3 T and even at 7 T on human scanners (89).

When it comes to clinical translation, the most powerful aspect of CEST MRI is the availability of endogenous agents in the proton exchange family. Already in 2000, shortly after the initial CEST article, Dagher et al. (132) were able to image urea in the kidney at a field of 1.5 T (Fig. 12a). A few years later, Zhou et al. (25) showed that the amide protons of mobile proteins and peptides previously characterized in vivo using WEX spectroscopy [Fig. 6b,c, (49,50)] could also be detected indirectly through the water signal using CEST. This amide proton transfer (APT) MRI was subsequently used to image early ischemia in anesthetized rats [Fig. 12b, (25,70)], where a pH reduction slows the exchange between the amide and water protons, leading to a reduction in CEST contrast (Fig. 7e–f). Such pH contrast seems particularly useful during the very early stages of ischemia where T_1, T_2, or diffusion weighted images may not yet show contrast, but where a pH penumbra may indicate risk for infarction due to impaired oxidative metabolism (Fig. 12b). Contrary to ^{31}P spectroscopy or WEX spectroscopy, APT has sufficient sensitivity to allow imaging and can be used under the standard clinical proton set up. APT-MRI is also showing potential for imaging cancer through an increase in cellular protein/peptide content of malignant cells with respect to normal tissue [Fig. 7a–c, (33)]. Cancer studies in animals indicate the ability to separate edema from tumor in animal (Fig. 7c), which has been confirmed in humans (82,107,108). These studies showed that APT can also detect non-enhancing high grade tumors. Recent human studies show preliminary suitability of APT for tumor grading [Fig. 12c, (82,108)], while animal studies on radiation necrosis models indicate the possibility to separate treatment effects from tumor progression (133). Another impressive example of endogenous CEST is the imaging of the OH group of glucosaminoglycans (gagCEST) in the human knee, which allowed detection of a lesion in the patella [Fig. 12d, (34)]. Measurements of gag concentration could be applied to diagnose gag-deficiency in tissue, such as expected to be the case in osteoarthritis. Another promising approach is the detection of OH-containing endogenous glycogen and glucose (26). These studies are somewhat complicated due to the chemical shift proximity of the OH resonances to the water protons, which hinders asymmetry analysis due to the artificial broadening of the bottom of the DS contribution to the Z-spectrum. This problem can be addressed with the aid of the WASSR approach (83), which allows such detection even at 3 T. GlycoCEST is expected to become more practical with the advent of human 7 T scanning (89,134–136), where the convolved CEST effects in the 0–5 ppm range downfield of water will be spread out more. In addition to the amide proton resonances of proteins and peptides, this region contains the effects of all exchangeable protons of in vivo metabolites and macromolecules resonating there, in a contribution depending

on their exchange rate (at physiological and other pH) and proton concentration. At higher field it may be possible to assign some of these, but due to the bandwidth of saturation, the linewidth of the resonances and the convolution of multiple contributing compounds, this will not be straightforward.

The availability of proton exchange as a contrast mechanism also offers the unique opportunity for using biodegradable natural compounds, such as sugars and proteins (26,29,130) as contrast agents. This seems to come close to the ideal of a totally noninvasive agent. Proteins may still have unknown toxicity though, and will have to be tested in careful trials. Their use currently has also been limited to animal studies (129,137). A nice example is the use of exchangeable protons in cationic polypeptides to both stabilize immunoprotective alginate microcapsules and

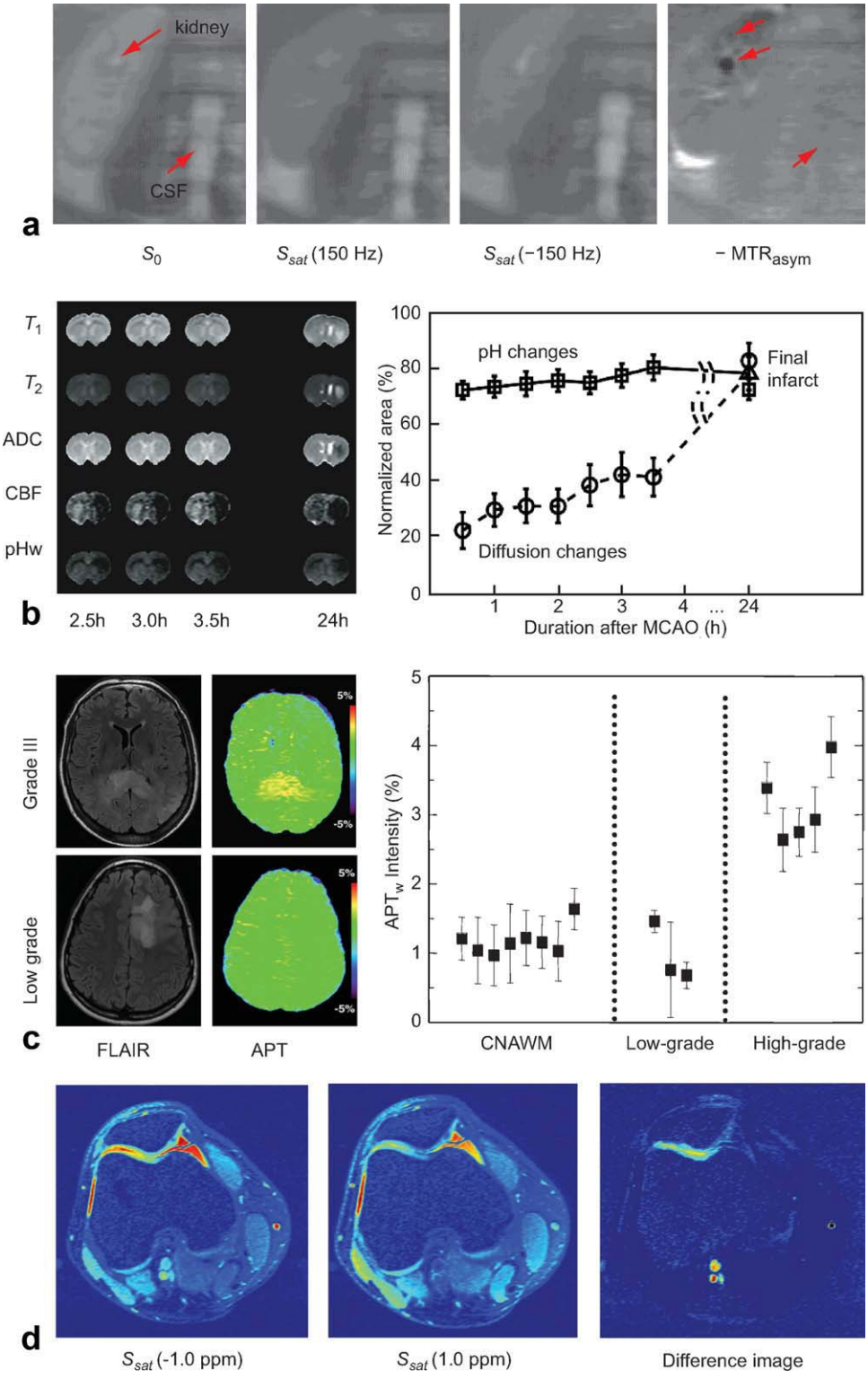

produce CEST contrast, allowing the monitoring of viability and functionality of encapsulated cells (138) as well as the distribution of cells and capsules in real-time (139). In addition to natural compounds, there is probably a large group of currently approved pharmaceuticals and contrast agents that contain exchangeable protons and can be employed immediately for CEST detection. A first example of this is discussed in a recent abstract by Liu et al. (124), who monitored cytosine deaminase activity for the conversion of the prodrug 5-Fluorocytosine (5-FC) into the active anti-tumor agent 5-fluorouracil (5-FU) through the difference in Z-spectra between 5-FC and 5-FU. Another example was presented by Longo et al. (103), who showed that the X-ray contrast agent iopamidol can be used to measure pH in vivo using the ratiomeric approach described earlier. Finally, the use of proton exchange instead of molecular exchange as the prime contrast in paramagnetic compounds is growing. A recent in vivo example of this is the monitoring of uptake of two different shift agents conjugated to fifth (G5) and second (G2) generation polyamidoamine (PAMAM) dendrimers in a mouse model of mammary carcinoma [MCF-7, (117)]. The results show a gradual increase of CEST contrast with time after injection, indicating an accumulation of the agent in the tumor.

With respect to paramagnetic exogenous agents, there is always the fear of toxicity, especially for metals becoming unbound and releasing into the tissue. However, chemistry is making rapid progress in the design of agents with both high thermodynamic and kinetic stability (140,141), the importance of the latter often being underestimated. Currently, there are exciting developments towards use of molecular exchange agents, both in vivo and ex vivo (perfused organs or cells). To the best of our knowledge, the first in vivo applications of paraCEST agents have been for the study of dynamic perfusion using the OPARACHEE approach of Vinogradov et al. (71). Figure 13a shows the uptake and clearance of a Tm-DOTAM-Gly compound in the mouse kidney, while Fig. 13b shows the uptake and retaining of a similar agent in a mouse Glioblastoma Multiforme tumor model (142). A limiting factor in the use of several paramagnetic molecular exchange compounds has been that T_1 and T_2 contrast is induced in addition to CEST contrast (143), although this can also be used to ones advantage (144). The 1–3% CEST contrast in the brain tumor model in Fig. 13b was corrected for the effects of relaxation. A very beautiful study highlighting the power of paraCEST agents for molecular sensing was recently performed by Ren et al. (145), who used the compound Europium(III)-1,4,7,10-tetraazacyclododecane-1,7-di-*N*-methylacetamide-4-10-di-*N*(m-phenylborate)acetamide (Eu-D2MA-2PB), which preferably binds glucose over coordinating water (106). Mouse livers containing the glucose sensor showed a 17% increase in CEST contrast when comparing perfusion with glucose to perfusion without glucose at a field of 4.7 T (Fig. 13c). Overall, the paraCEST approach is very promising because of the clean excitation of resonances without much direct water saturation. The disadvantage of the need for high power deposition (inducing strong MTC) may perhaps be overcome with the new FLEX method. The combination proton exchange and molecular exchange paramagnetic compounds offers an order of magnitude increase in sensitivity as well as the use of two sensors with different chemical shift in a single molecule (146).

Based on the potential of high payload, the development of compartmental exchange agents for use in vivo is very important. Recently, the first studies demonstrating the use of paraCEST-based and diaCEST-based liposomes in vivo were reported. In a study employing multiple types of paramagnetic contrast in two types of liposomes (mixed paraCEST/T_2 liposome and mixed T_1/T_2 liposome), Delli Castelli et al. (95) were able to use the CEST contrast to monitor endocytosis of the CEST liposomes in the cells, which reduced the CEST contrast (Fig. 14a). This study combined the CEST images with T_1 and T_2 maps to build a kinetic model for the fate of the paramagnetic complexes loaded into the liposomes. In another study Liu et al. (129) demonstrated the use of

FIG. 12. In vivo CEST studies exploiting the presence of endogenous proton exchange agents. **a:** Imaging of urea in kidney. Comparison of coronal images through the kidney of a normal volunteer kidney without saturation (S_0), and with saturation (S_{sat}) applied symmetrically about the water frequency for the resonance frequency difference (+150 Hz at 1.5 T) of urea protons. The red arrows in the S_0 image indicate the calyx in the kidney (urea collecting system) and CSF in the spinal cord, which is used as a reference. The asymmetry image on the right is inverse of current definition and therefore labeled as $-MTR_{asym}$. This image is darker in the calyx (middle red arrow) and renal papillae (top arrow) while no differences are visible in CSF (bottom arrow). Reproduced with permission from Dagher et al., J Magn Reson Imaging 2000;12:745-748. **b:** Imaging of ischemia using pH dependence of APT MRI. Multiparametric MRI of rat brain as a function of time after permanent middle cerebral artery occlusion (MCAO). Early ischemia (as confirmed by cerebral blood flow weighted MRI) shows negligible changes in T_1, T_2, and ADC (apparent diffusion coefficient) images. However, a reduction in pH could be detected using APT-MRI (dubbed pHw), which predicted well evolution to stroke at 24 hrs, as confirmed by T_2-hyperintensity. In a series of 28 rats studied at 4.7 T, pH-weighted MRI predicted areas of infarction more accurately and earlier than diffusion MRI (graph). Reproduced with permission from Sun et al., J Cereb Blood Flow Metab 2007;27:1129-1136. **c:** Imaging of increased protein content in tumors using APT. FLAIR and APT images at 3 T for patients with a grade III (top) and a low grade (bottom) tumor. Contrast in FLAIR images appears similar for high and low grade. APT contrast, however, while increased by about 3% in the grade III tumor is virtually indistinguishable from contralateral normal-appearing white matter (CNAWM) in the low grade case, which was attributed to increased protein content with grade. This pilot study showed potential to separate high and low grade tumors for a small group (graph). Reproduced with permission from Zhou et al., Magn Reson Med 2008;60:842-849. **d:** GagCEST images at 1.5 T of cartilage lesion on the medial facet of the patellofemoral human knee joint. Left: patella with irradiation at −1.0 ppm and 1 ppm (corresponding to OH protons, see Fig. 5). The MTR_{asym} image shows CEST contrast from the femur and the lateral and medial sides of the patella. A loss of gagCEST is clear. The bright circular sections highlight the location of blood vessels, was attributed to the CEST effect from oligosaccharides and proteins in blood. Reproduced with permission from Ling et al., Proc Natl Acad Sci USA 2008;105:2266–2270. Color image provided by Alexej Jerschow. [Color figure can be viewed in the online issue, which is available at wileyonlinelibrary.com.]

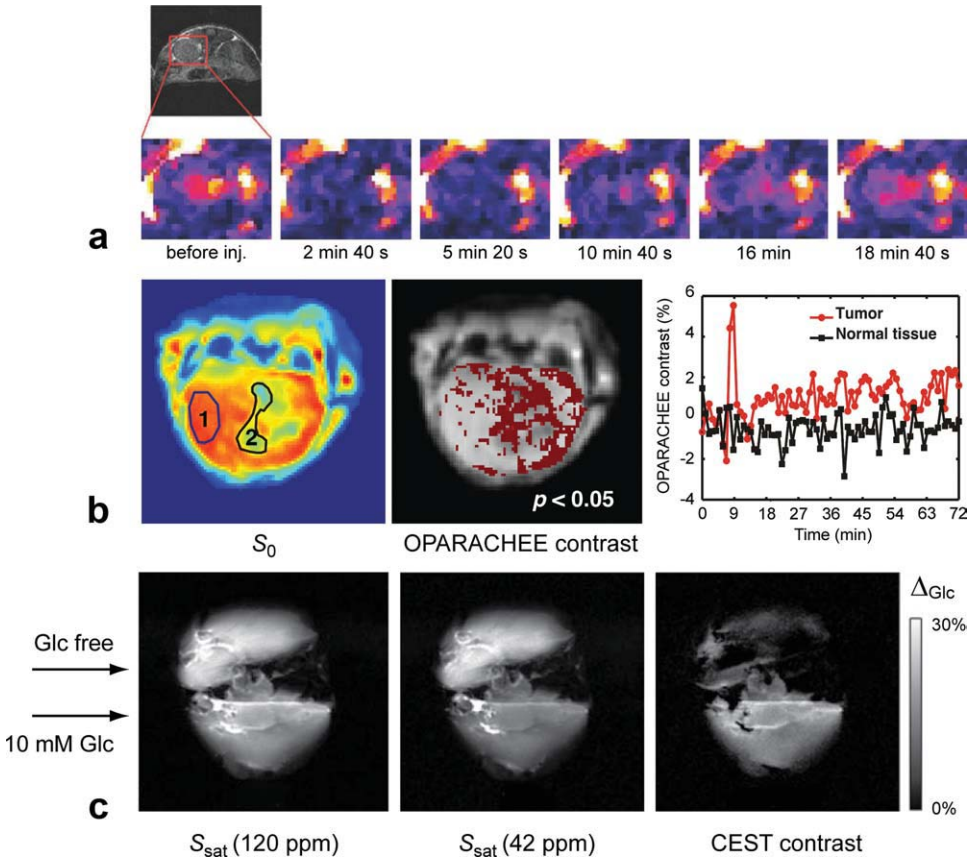

FIG. 13. In vivo and ex vivo CEST studies of molecular exchange compounds. **a, b:** paraCEST perfusion imaging in vivo. a: Kidney perfusion study by Vinogradov, showing CEST images before, during and after injection of Tm-DOTAM-Gly, with hypointensity when the agent reaches the kidney. Reproduced with permission from Vinogradev et al., Magn Reson Med 2007;58:650-655. b: Brain and glioblastoma perfusion study using Tm-DOTAM-Gly-Lys. Left: Flash image for region assignment of healthy tissue (1) and tumor (2). Right: Dynamic signal changes before, during and after perfusion, showing that some agent is retained in the leaky tumors, but not in brain. Middle: significantly changed CEST contrast in regions roughly corresponding to tumor. Reproduced with permission from Li et al., Proceedings of the 18th Annual Meeting of ISMRM, Stockholm, Sweden, 2010. p 3752. **c:** Glucose sensing ex vivo using paraCEST agents. MRI images of two mouse livers, one perfused with Eu-D2MA-2PB solution containing glucose (Bottom) and another without glucose (Top). CEST contrast is clear in the liver perfused with glucose only. Reproduced with permission from Ren et al., Magn Reson Med 2008;60:1047–1055.

"multicolor" mixtures of liposomes loaded with proton exchange agents such as glycogen (Glyc), poly-L-lysine (PLL), and L-arginine (Larg), in which the different chemical shifts of the exchangeable protons (OH, NH and NH_2, respectively) were assigned different colors (130) in analogy to optical imaging. Each liposome type displayed a characteristic MTR_{asym} plot in vitro (Fig. 14b, LEFT). Depending on the diaCEST agent used, the intraparticle exchange rate is not as fast as for paraCEST liposomes and the contrast is probably a mixture of proton exchange and compartmental exchange. When injecting PLL and Larg in the two footpads of mice, signal was found in the ipsilateral regional lymph nodes, showing that transport of these liposomes can be monitored in vivo. In addition, the in vivo MTR_{asym} -spectra (Fig. 14b, RIGHT) resembled the in vitro reference data. From a mechanistic point of view, this diamagnetic approach should be less sensitive than paramagnetic lipoCEST because exchange is slower and protons have to be transferred from the agent to the water inside the liposome (smaller pool) in an additional exchange step that is on the order of magnitude of the compartmental exchange rate (10–200 Hz). If this rate were to be increased, the labeling efficiency would go down or the power demands up, which is not the case for paramagnetic lipoCEST. On the other hand, the original chemical shift of the agent can be used, allowing good separation from the water signal. However, the small shift in paramagnetic liposomes can be increased tremendously by increasing the bulk magnetic susceptibility contributions to the shift through making the particles magnetically anisotropic (113). Both approaches have great possibilities though, and the multifrequency and multicontrast approaches employed in these two studies show only a preliminary glimpse into the promising world of lipoCEST imaging.

CONCLUSION

The discovery of the CEST effect has added a new dimension to the design and detection of MRI contrast agents both with respect to the chemistry involved and

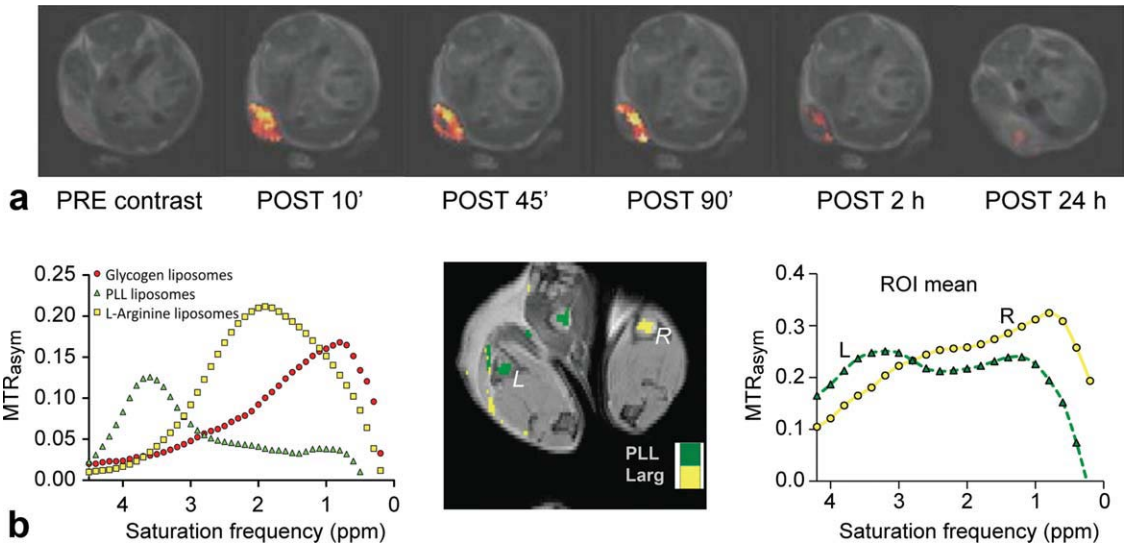

FIG. 14. In vivo CEST studies using compartmental exchange agents. **a:** Paramagnetic lipoCEST MRI. Temporal evolution of CEST contrast after injecting a compartmental exchange agent loaded with Tm-DOTA into the tumor of a murine melanoma model. CEST contrast is lost about 2 hours after administering the compartmental exchange agent, indicating uptake by the cell and removal of the liposome membrane. Reproduced with permission from Delli Castelli et al., J Controlled Release 2010;144:271-279. **b:** Diamagnetic lipoCEST MRI. Left: MTR_{asym} plot showing the water signal intensity reduction as a function of frequency for three diamagnetic liposomes (DLs) at about 30 nM concentration in vitro (pH = 7.3 and 37°C), with red assigned to OH in Glyc DL, yellow assigned to NH_2 in Larg DL, and green assigned to NH in PLL DL. Middle: MRI images of regional lymph nodes in mice showing two-color CEST contrast after being injected with liposomes containing PLL and Larg in left (L) and right (R) footpads, respectively, 24 hours before MRI. Right: mean MTR_{asym} plots of the left (*L*) and right (*R*) lymph nodes. Courtesy of Guanshu Liu and Michael McMahon, Kennedy Krieger Institute and Johns Hopkins University School of Medicine. [Color figure can be viewed in the online issue, which is available at wileyonlinelibrary.com.]

the new MRI technology that can be employed. From a chemistry point of view, the exchange transfer principle has allowed the design of whole new groups of contrast agents. These range from powerful paramagnetic shift agents with multiple functions to simple biodegradable compounds such as peptides and sugars, which have great potential as truly noninvasive contrast agents. Contrary to relaxation agents, exchange transfer contrast can be turned on and off, and compounds can be designed to contain protons that resonate at multiple frequencies, expanding the MRI field to a multicolor type of imaging in analogy to optical imaging. In addition to exogenous agents, many endogenous compounds show CEST contrast, which can be exploited as inherent biomarkers for detection of disease and monitoring of the effects of treatment. In this brief review, we have highlighted mainly the MR-methodological aspects of exchange transfer, which indicate that we are only scratching the surface of possible approaches. Current MR methods have focused mainly on saturation transfer, while a whole new field of multidimensional MR approaches to detect exchange-transfer and cross-relaxation aspects of the contrast remains to be explored. In addition to many chemical advances, we therefore foresee that much new MRI technology will be developed in the coming years, which will rapidly expand this exciting field of research.

ACKNOWLEDGMENTS

The authors are grateful to Dr. Alexej Jerschow (New York University), Dr. Robert Bartha (Robarts Research Institute, London, Ontario), Dr. Mark Woods (Portland State University, Portland), Dr. Dean Sherry (University of Texas, Southwestern Medical Center, Dallas), Dr. Guanshu Liu, Dr. Mike McMahon, and Dr. Josh Friedman for providing some of the figures and Dr. Mike McMahon and Dr. Manus Donahue for carefully reading the paper. The National Center for Research Resources (NCRR) is a component of the National Institutes of Health (NIH). The contents of the paper are solely the responsibility of the authors and do not necessarily represent the official view of NCRR or NIH.

REFERENCES

1. Ward KM, Aletras AH, Balaban RS. A new class of contrast agents for MRI based on proton chemical exchange dependent saturation transfer (CEST). J Magn Reson 2000;143:79–87.
2. Zhang S, Merritt M, Woessner DE, Lenkinski RE, Sherry AD. PARACEST agents: modulating MRI contrast via water proton exchange. Acc Chem Res 2003; 36:783–790.
3. Woods M, Woessner DE, Sherry AD. Paramagnetic lanthanide complexes as PARACEST agents for medical imaging. Chem Soc Rev 2006;35:500–511.
4. Zhou J, van Zijl P. Chemical exchange saturation transfer imaging and spectroscopy. Prog Nucl Magn Reson Spectrosc 2006;48:109–136.
5. Sherry AD, Woods M. Chemical exchange saturation transfer contrast agents for magnetic resonance imaging. Annu Rev Biomed Eng 2008;10:391–411.
6. Terreno E, Delli Castelli D, Cabella C, Dastru W, Sanino A, Stancanello J, Tei L, Aime S. Paramagnetic liposomes as innovative contrast agents for magnetic resonance (MR) molecular imaging applications. Chem Biodivers 2008;5:1901–1912.
7. Aime S, Castelli DD, Terreno E. Chapter 10—lanthanide-loaded paramagnetic liposomes as switchable magnetically oriented nanovesicles. Methods Enzymol 2009;464:193–210.

8. Terreno E, Stancanello J, Longo D, Castelli DD, Milone L, Sanders HM, Kok MB, Uggeri F, Aime S. Methods for an improved detection of the MRI-CEST effect. Contrast Media Mol Imaging 2009;4:237–247.
9. Hancu I, Dixon WT, Woods M, Vinogradov E, Sherry AD, Lenkinski RE. CEST and PARACEST MR contrast agents. Acta Radiol 2010;51: 910–923.
10. Terreno E, Castelli DD, Aime S. Encoding the frequency dependence in MRI contrast media: the emerging class of CEST agents. Contrast Media Mol Imaging 2010;5:78–98.
11. Terreno E, Castelli DD, Viale A, Aime S. Challenges for molecular magnetic resonance imaging. Chem Rev 2010;110:3019–3042.
12. Wolff SD, Balaban RS. Magnetization transfer contrast (MTC) and tissue water proton relaxation in vivo. Magn Reson Med 1989;10: 135–144.
13. Bryant RG. The dynamics of water-protein interactions. Annu Rev Biophys Biomol Struct 1996;25:29–53.
14. Guivel-Scharen V, Sinnwell T, Wolff SD, Balaban RS. Detection of proton chemical exchange between metabolites and water in biological tissues. J Magn Reson 1998;133:36–45.
15. Forsen S, Hoffman RA. Study of moderately rapid chemical exchange reactions by means of nuclear magnetic double resonance. J Chem Phys 1963;39:2892–2901.
16. Li AX, Hudson RH, Barrett JW, Jones CK, Pasternak SH, Bartha R. Four-pool modeling of proton exchange processes in biological systems in the presence of MRI-paramagnetic chemical exchange saturation transfer (PARACEST) agents. Magn Reson Med 2008;60: 1197–1206.
17. McConnell HM. Reaction rates by nuclear magnetic resonance. J Chem Phys 1958;28:430–431.
18. McMahon MT, Gilad AA, Zhou J, Sun PZ, Bulte JW, van Zijl PC. Quantifying exchange rates in chemical exchange saturation transfer agents using the saturation time and saturation power dependencies of the magnetization transfer effect on the magnetic resonance imaging signal (QUEST and QUESP): pH calibration for poly-L-lysine and a starburst dendrimer. Magn Reson Med 2006;55:836–847.
19. Sun PZ. Simplified and scalable numerical solution for describing multi-pool chemical exchange saturation transfer (CEST) MRI contrast. J Magn Reson 2010;205:235–241.
20. Sun PZ, Zhou J, Huang J, van Zijl P. Simplified quantitative description of amide proton transfer (APT) imaging during acute ischemia. Magn Reson Med 2007;57:405–410.
21. Woessner DE. Nuclear transfer effects in nuclear magnetic resonance pulse experiments. J Chem Phys 1961;35:41–48.
22. Woessner DE, Zhang S, Merritt ME, Sherry AD. Numerical solution of the Bloch equations provides insights into the optimum design of PARACEST agents for MRI. Magn Reson Med 2005;53:790–799.
23. Zhou J, Wilson DA, Sun PZ, Klaus JA, Van Zijl PC. Quantitative description of proton exchange processes between water and endogenous and exogenous agents for WEX, CEST, and APT experiments. Magn Reson Med 2004;51:945–952.
24. Snoussi K, Bulte JW, Gueron M, van Zijl PC. Sensitive CEST agents based on nucleic acid imino proton exchange: detection of poly(rU) and of a dendrimer-poly(rU) model for nucleic acid delivery and pharmacology. Magn Reson Med 2003;49:998–1005.
25. Zhou J, Payen JF, Wilson DA, Traystman RJ, van Zijl PC. Using the amide proton signals of intracellular proteins and peptides to detect pH effects in MRI. Nat Med 2003;9:1085–1090.
26. van Zijl PC, Jones CK, Ren J, Malloy CR, Sherry AD. MRI detection of glycogen in vivo by using chemical exchange saturation transfer imaging (glycoCEST). Proc Natl Acad Sci USA 2007;104:4359–4364.
27. Aime S, Barge A, Delli Castelli D, Fedeli F, Mortillaro A, Nielsen FU, Terreno E. Paramagnetic lanthanide(III) complexes as pH-sensitive chemical exchange saturation transfer (CEST) contrast agents for MRI applications. Magn Reson Med 2002;47:639–648.
28. Aime S, Delli Castelli D, Fedeli F, Terreno E. A paramagnetic MRI-CEST agent responsive to lactate concentration. J Am Chem Soc 2002;124:9364–9365.
29. Zhang S, Trokowski R, Sherry AD. A paramagnetic CEST agent for imaging glucose by MRI. J Am Chem Soc 2003;125:15288–15289.
30. Zhang S, Winter P, Wu K, Sherry AD. A novel europium(III)-based MRI contrast agent. J Am Chem Soc 2001;123:1517–1518.
31. Goffeney N, Bulte JW, Duyn J, Bryant LH, Jr, van Zijl PC. Sensitive NMR detection of cationic-polymer-based gene delivery systems using saturation transfer via proton exchange. J Am Chem Soc 2001; 123:8628–8629.
32. Ward KM, Balaban RS. Determination of pH using water protons and chemical exchange dependent saturation transfer (CEST). Magn Reson Med 2000;44:799–802.
33. Zhou J, Lal B, Wilson DA, Laterra J, van Zijl PC. Amide proton transfer (APT) contrast for imaging of brain tumors. Magn Reson Med 2003;50:1120–1126.
34. Ling W, Regatte RR, Navon G, Jerschow A. Assessment of glycosaminoglycan concentration in vivo by chemical exchange-dependent saturation transfer (gagCEST). Proc Natl Acad Sci USA 2008; 105:2266–2270.
35. Aime S, Delli Castelli D, Terreno E. Highly sensitive MRI chemical exchange saturation transfer agents using liposomes. Angew Chem Int Ed 2005;44:5513–5515.
36. Friedman JI, McMahon MT, Stivers JT, van Zijl PC. Indirect detection of labile solute proton spectra via the water signal using frequency-labeled exchange (FLEX) transfer. J Am Chem Soc 2010;132: 1813–1815.
37. Schroder L, Lowery TJ, Hilty C, Wemmer DE, Pines A. Molecular imaging using a targeted magnetic resonance hyperpolarized biosensor. Science 2006;314:446–449.
38. Zhao JM, Har-el YE, McMahon MT, Zhou J, Sherry AD, Sgouros G, Bulte JW, van Zijl PC. Size-induced enhancement of chemical exchange saturation transfer (CEST) contrast in liposomes. J Am Chem Soc 2008;130:5178–5184.
39. Liepinsh E, Otting G. Proton exchange rates from amino acid side chains—implications for image contrast. Magn Reson Med 1996;35:30–42.
40. Viswanathan S, Kovacs Z, Green KN, Ratnakar SJ, Sherry AD. Alternatives to gadolinium-based metal chelates for magnetic resonance imaging. Chem Rev 2010;110:2960–3018.
41. Ratnakar SJ, Woods M, Lubag AJ, Kovacs Z, Sherry AD. Modulation of water exchange in europium(III) DOTA-tetraamide complexes via electronic substituent effects. J Am Chem Soc 2008;130:6–7.
42. Cavanagh J, Fairbrother WJ, Palmer III AF, Skelton NJ. Protein NMR spectroscopy: principles and practice. San Diego: Academic Press; 1996.
43. Ernst RR, Bodenhausen G, Wokaun A. Principles of nuclear magnetic resonance in one and two dimensions. Oxford: Oxford University Press; 1988.
44. Wüthrich K. NMR of proteins and nucleic acids. New York: Wiley; 1986.
45. Ling W, Eliav U, Navon G, Jerschow A. Chemical exchange saturation transfer by intermolecular double-quantum coherence. J Magn Reson 2008;194:29–32.
46. Hwang TL, van Zijl PC, Mori S. Accurate quantitation of water-amide proton exchange rates using the phase-modulated CLEAN chemical EXchange (CLEANEX-PM) approach with a Fast-HSQC (FHSQC) detection scheme. J Biomol NMR 1998;11:221–226.
47. Mori S, Abeygunawardana C, van Zijl PC, Berg JM. Water exchange filter with improved sensitivity (WEX II) to study solvent-exchangeable protons. Application to the consensus zinc finger peptide CP-1. J Magn Reson B 1996;110:96–101.
48. Mori S, O'Neil Johnson M, Berg JM, van Zijl PC. A water exchange filter (WEX-filter) for NMR studies of macromolecules. J Am Chem Soc 1994;116:11982–11984.
49. Mori S, Eleff SM, Pilatus U, Mori N, van Zijl PC. Proton NMR spectroscopy of solvent-saturable resonances: a new approach to study pH effects in situ. Magn Reson Med 1998;40:36–42.
50. van Zijl PC, Zhou J, Mori N, Payen JF, Wilson D, Mori S. Mechanism of magnetization transfer during on-resonance water saturation. A new approach to detect mobile proteins, peptides, and lipids. Magn Reson Med 2003;49:440–449.
51. Otting G, Liepinsh E, Wuthrich K. Protein hydration in aqueous solution. Science 1991;254:974–980.
52. Hua J, Jones CK, Blakeley J, Smith SA, van Zijl PC, Zhou J. Quantitative description of the asymmetry in magnetization transfer effects around the water resonance in the human brain. Magn Reson Med 2007;58:786–793.
53. Pekar J, Jezzard P, Roberts DA, Leigh JS, Jr., Frank JA, McLaughlin AC. Perfusion imaging with compensation for asymmetric magnetization transfer effects. Magn Reson Med 1996;35:70–79.
54. Swanson S, Pang Y. MT is symmetric but shifted with respect to water. In: Proceedings of the 11th Annual Meeting of ISMRM, Ontario, Canada 2003. p 660.
55. Englander SW, Kallenbach NR. Hydrogen exchange and structural dynamics of proteins and nucleic acids. Q Rev Biophys 1984;16: 521–655.

56. Gillies RJ, Raghunand N, Garcia-Martin ML, Gatenby RA. pH imaging. A review of pH measurement methods and applications in cancers. IEEE Eng Med Biol Mag 2004;23:57–64.
57. Griffiths JR. Are cancer cells acidic? Br J Cancer 1991;64:425–427.
58. Balaban RS, Ceckler TL. Magnetization transfer contrast in magnetic resonance imaging. Magn Reson Q 1992;8:116–137.
59. Henkelman RM, Huang X, Xiang QS, Stanisz GJ, Swanson SD, Bronskill MJ. Quantitative interpretation of magnetization transfer. Magn Reson Med 1993;29:759–766.
60. Henkelman RM, Stanisz GJ, Graham SJ. Magnetization transfer in MRI: a review. NMR Biomed 2001;14:57–64.
61. Leibfritz D, Dreher W. Magnetization transfer MRS. NMR Biomed 2001;14:65–76.
62. McGowan JC, III, Schnall MD, Leigh JS. Magnetization transfer imaging with pulsed off-resonance saturation: variation in contrast with saturation duty cycle. J Magn Reson Imaging 1994;4:79–82.
63. Pike GB. Pulsed magnetization transfer contrast in gradient echo imaging: a two-pool analytic description of signal response. Magn Reson Med 1996;36:95–103.
64. Pike GB, Glover GH, Hu BS, Enzmann DR. Pulsed magnetization transfer spin-echo MR imaging. J Magn Reson Imaging 1993;3:531–539.
65. Graham SJ, Henkelman RM. Understanding pulsed magnetization transfer. J Magn Reson Imaging 1997;7:903–912.
66. Hu BS, Conolly SM, Wright GA, Nishimura DG, Macovski A. Pulsed saturation transfer contrast. Magn Reson Med 1992;26:231–240.
67. Yeung HN, Aisen AM. Magnetization transfer contrast with periodic pulsed saturation. Radiology 1992;183:209–214.
68. Gochberg DF, Gore JC. Quantitative imaging of magnetization transfer using an inversion recovery sequence. Magn Reson Med 2003; 49:501–505.
69. Sun PZ, Benner T, Kumar A, Sorensen AG. Investigation of optimizing and translating pH-sensitive pulsed-chemical exchange saturation transfer (CEST) imaging to a 3T clinical scanner. Magn Reson Med 2008;60:834–841.
70. Sun PZ, Zhou J, Sun W, Huang J, van Zijl PC. Detection of the ischemic penumbra using pH-weighted MRI. J Cereb Blood Flow Metab 2007;27:1129–1136.
71. Vinogradov E, He H, Lubag A, Balschi JA, Sherry AD, Lenkinski RE. MRI detection of paramagnetic chemical exchange effects in mice kidneys in vivo. Magn Reson Med 2007;58:650–655.
72. Vinogradov E, Zhang S, Lubag A, Balschi JA, Sherry AD, Lenkinski RE. On-resonance low B_1 pulses for imaging of the effects of PARACEST agents. J Magn Reson 2005;176:54–63.
73. Eliav U, Navon G. Enhancement of magnetization transfer effects by inter-molecular multiple quantum filtered NMR. J Magn Reson 2008;190:149–153.
74. Warren WS, Richter W, Andreotti AH, Farmer BT, II. Generation of impossible cross-peaks between bulk water and biomolecules in solution NMR. Science 1993;262:2005–2009.
75. Zhang S, Zhu X, Chen Z, Cai C, Lin T, Zhong J. Improvement in the contrast of CEST MRI via intermolecular double quantum coherences. Phys Med Biol 2008;53:N287–296.
76. Ropele S, Stollberger R, Hartung HP, Fazekas F. Estimation of magnetization transfer rates from PACE experiments with pulsed RF saturation. J Magn Reson Imaging 2000;12:749–756.
77. Sled JG, Pike GB. Quantitative imaging of magnetization transfer exchange and relaxation properties in vivo using MRI. Magn Reson Med 2001;46:923–931.
78. Yarnykh VL. Pulsed Z-spectroscopic imaging of cross-relaxation parameters in tissues for human MRI: theory and clinical applications. Magn Reson Med 2002;47:929–939.
79. Atreya HS, Szyperski T. Rapid NMR data collection. Methods Enzymol 2005;394:78–108.
80. Frydman L, Scherf T, Lupulescu A. The acquisition of multidimensional NMR spectra within a single scan. Proc Natl Acad Sci USA 2002;99:15858–15862.
81. Mobli M, Stern AS, Hoch JC. Spectral reconstruction methods in fast NMR: reduced dimensionality, random sampling and maximum entropy. J Magn Reson 2006;182:96–105.
82. Zhou J, Blakeley JO, Hua J, Kim M, Laterra J, Pomper MG, van Zijl PC. Practical data acquisition method for human brain tumor amide proton transfer (APT) imaging. Magn Reson Med 2008;60:842–849.
83. Kim M, Gillen J, Landman BA, Zhou J, van Zijl PC. Water saturation shift referencing (WASSR) for chemical exchange saturation transfer (CEST) experiments. Magn Reson Med 2009;61:1441–1450.
84. Mulkern RV, Williams ML. The general solution to the Bloch equation with constant rf and relaxation terms: application to saturation and slice selection. Med Phys 1993;20:5–13.
85. Metzger GJ, Snyder C, Akgun C, Vaughan T, Ugurbil K, Van de Moortele PF. Local B_1^+ shimming for prostate imaging with transceiver arrays at 7T based on subject-dependent transmit phase measurements. Magn Reson Med 2008;59:396–409.
86. Setsompop K, Alagappan V, Zelinski AC, Potthast A, Fontius U, Hebrank F, Schmitt F, Wald LL, Adalsteinsson E. High-flip-angle slice-selective parallel RF transmission with 8 channels at 7 T. J Magn Reson 2008;195:76–84.
87. Zhu H, Jones CK, van Zijl PC, Barker PB, Zhou J. Fast 3D chemical exchange saturation transfer (CEST) imaging of the human brain. Magn Reson Med 2010;64:638–644.
88. Dixon WT, Hancu I, Ratnakar SJ, Sherry AD, Lenkinski RE, Alsop DC. A multislice gradient echo pulse sequence for CEST imaging. Magn Reson Med 2010;63:253–256.
89. Mougin OE, Coxon RC, Pitiot A, Gowland PA. Magnetization transfer phenomenon in the human brain at 7 T. NeuroImage 2010;49: 272–281.
90. Sun PZ, Murata Y, Lu J, Wang X, Lo EH, Sorensen AG. Relaxation-compensated fast multislice amide proton transfer (APT) imaging of acute ischemic stroke. Magn Reson Med 2008;59:1175–1182.
91. Sun PZ, Zhou J, Sun W, Huang J, van Zijl PC. Suppression of lipid artifacts in amide proton transfer imaging. Magn Reson Med 2005; 54:222–225.
92. Dixon WT, Ren J, Lubag AJ, Ratnakar J, Vinogradov E, Hancu I, Lenkinski RE, Sherry AD. A concentration-independent method to measure exchange rates in PARACEST agents. Magn Reson Med 2010; 63:625–632.
93. Aime S, Delli Castelli D, Terreno E. Novel pH-reporter MRI contrast agents. Angew Chem Int Ed 2002;41:4334–4336.
94. Terreno E, Delli Castelli D, Cravotto G, Milone L, Aime S. Ln(III)-DOTAMGly complexes: a versatile series to assess the determinants of the efficacy of paramagnetic chemical exchange saturation transfer agents for magnetic resonance imaging applications. Invest Radiol 2004;39:235–243.
95. Delli Castelli D, Dastru W, Terreno E, Cittadino E, Mainini F, Torres E, Spadaro M, Aime S. In vivo MRI multicontrast kinetic analysis of the uptake and intracellular trafficking of paramagnetically labeled liposomes. J Controlled Release 2010;144:271–279.
96. Burdinski D, Pikkemaat JA, Lub J, de Peinder P, Nieto Garrido L, Weyhermuller T. Lanthanide complexes of triethylenetetramine tetra-, penta-, and hexaacetamide ligands as paramagnetic chemical exchange-dependent saturation transfer contrast agents for magnetic resonance imaging: nona- versus decadentate coordination. Inorg Chem 2009;48:6692–6712.
97. Huang CH, Hammell J, Ratnakar SJ, Sherry AD, Morrow JR. Activation of a PARACEST agent for MRI through selective outersphere interactions with phosphate diesters. Inorg Chem 2010;49: 5963–5970.
98. Huang CH, Morrow JR. A PARACEST agent responsive to inner- and outer-sphere phosphate ester interactions for MRI applications. J Am Chem Soc 2009;131:4206–4207.
99. Huang CH, Morrow JR. Cerium(III), europium(III), and ytterbium(III) complexes with alcohol donor groups as chemical exchange saturation transfer agents for MRI. Inorg Chem 2009;48:7237–7243.
100. Perez-Mayoral E, Negri V, Soler-Padros J, Cerdan S, Ballesteros P. Chemistry of paramagnetic and diamagnetic contrast agents for magnetic resonance imaging and spectroscopy pH responsive contrast agents. Eur J Radiol 2008;67:453–458.
101. Pikkemaat JA, Wegh RT, Lamerichs R, van de Molengraaf RA, Langereis S, Burdinski D, Raymond AY, Janssen HM, de Waal BF, Willard NP, Meijer EW, Grull H. Dendritic PARACEST contrast agents for magnetic resonance imaging. Contrast Media Mol Imaging 2007; 2:229–239.
102. Sun PZ, Sorensen AG. Imaging pH using the chemical exchange saturation transfer (CEST) MRI: correction of concomitant RF irradiation effects to quantify CEST MRI for chemical exchange rate and pH. Magn Reson Med 2008;60:390–397.
103. Longo DL, Dastru W, Digilio G, Keupp J, Langereis S, Lanzardo S, Prestigio S, Steinbach O, Terreno E, Uggeri F, Aime S. Iopamidol as a responsive MRI-chemical exchange saturation transfer contrast agent for pH mapping of kidneys: in vivo studies in mice at 7T. Magn Reson Med 2011;65:202–211.

104. Aime S, Barge A, Cabella C, Crich SG, Gianolio E. Targeting cells with MR imaging probes based on paramagnetic Gd(III) chelates. Curr Pharm Biotechnol 2004;5:509–518.
105. Liu G, Li Y, Pagel MD. Design and characterization of a new irreversible responsive PARACEST MRI contrast agent that detects nitric oxide. Magn Reson Med 2007;58:1249–1256.
106. Trokowski R, Zhang S, Sherry AD. Cyclen-based phenylboronate ligands and their Eu^{3+} complexes for sensing glucose by MRI. Bioconjug Chem 2004;15:1431–1440.
107. Jones CK, Schlosser MJ, van Zijl PC, Pomper MG, Golay X, Zhou J. Amide proton transfer imaging of human brain tumors at 3T. Magn Reson Med 2006;56:585–592.
108. Wen Z, Hu S, Huang F, Wang X, Guo L, Quan X, Wang S, Zhou J. MR imaging of high-grade brain tumors using endogenous protein and peptide-based contrast. NeuroImage 2010;51:616–622.
109. Angelovski G, Chauvin T, Pohmann R, Logothetis NK, Toth E. Calcium-responsive paramagnetic CEST agents. Bioorg Med Chem 2010; doi: 10.1016/j.bmc.2010.07.023.
110. Trokowski R, Ren J, Kalman FK, Sherry AD. Selective sensing of zinc ions with a PARACEST contrast agent. Angew Chem Int Ed 2005;44:6920–6923.
111. Aime S, Delli Castelli D, Lawson D, Terreno E. Gd-loaded liposomes as T_1, susceptibility, and CEST agents, all in one. J Am Chem Soc 2007;129:2430–2431.
112. Terreno E, Castelli DD, Milone L, Rollet S, Stancanello J, Violante E, Aime S. First ex-vivo MRI co-localization of two LIPOCEST agents. Contrast Media Mol Imaging 2008;3:38–43.
113. Terreno E, Delli Castelli D, Violante E, Sanders HM, Sommerdijk NA, Aime S. Osmotically shrunken LIPOCEST agents: an innovative class of magnetic resonance imaging contrast media based on chemical exchange saturation transfer. Chemistry 2009;15:1440–1448.
114. Vasalatiy O, Gerard RD, Zhao P, Sun X, Sherry AD. Labeling of adenovirus particles with PARACEST agents. Bioconjug Chem 2008;19: 598–606.
115. Aime S, Delli Castelli D, Terreno E. Supramolecular adducts between poly-L-arginine and [TmIIIdotp]: a route to sensitivity-enhanced magnetic resonance imaging-chemical exchange saturation transfer agents. Angew Chem Int Ed 2003;42:4527–4529.
116. Ali MM, Liu G, Shah T, Flask CA, Pagel MD. Using two chemical exchange saturation transfer magnetic resonance imaging contrast agents for molecular imaging studies. Acc Chem Res 2009;42: 915–924.
117. Ali MM, Yoo B, Pagel MD. Tracking the relative in vivo pharmacokinetics of nanoparticles with PARACEST MRI. Mol Pharmaceutics 2009;6:1409–1416.
118. Ali MM, Woods M, Suh EH, Kovacs Z, Tircso G, Zhao P, Kodibagkar VD, Sherry AD. Albumin-binding PARACEST agents. J Biol Inorg Chem 2007;12:855–865.
119. Nwe K, Andolina CM, Huang CH, Morrow JR. PARACEST properties of a dinuclear neodymium(III) complex bound to DNA or carbonate. Bioconjug Chem 2009;20:1375–1382.
120. Langereis S, Keupp J, van Velthoven JL, de Roos IH, Burdinski D, Pikkemaat JA, Grull H. A temperature-sensitive liposomal ^{1}H CEST and ^{19}F contrast agent for MR image-guided drug delivery. J Am Chem Soc 2009;131:1380–1381.
121. Li AX, Wojciechowski F, Suchy M, Jones CK, Hudson RH, Menon RS, Bartha R. A sensitive PARACEST contrast agent for temperature MRI: Eu^{3+}-DOTAM-glycine (Gly)-phenylalanine (Phe). Magn Reson Med 2008;59:374–381.
122. Zhang S, Malloy CR, Sherry AD. MRI thermometry based on PARACEST agents. J Am Chem Soc 2005;127:17572–17573.
123. Chauvin T, Durand P, Bernier M, Meudal H, Doan BT, Noury F, Badet B, Beloeil JC, Toth E. Detection of enzymatic activity by PARACEST MRI: a general approach to target a large variety of enzymes. Angew Chem Int Ed 2008;47:4370–4372.
124. Liu G, Bernard SM, Tse T, Walczak P, McMahon MT, Bulte JW, van Zijl PCM, Gilad AA. Direct detection of cytosine deaminase enzymatic activity using CEST MRI. In: Proceedings of the 18th Annual Meeting of ISMRM, Stockholm, Sweden 2010. p 36.
125. Yoo B, Pagel MD. A PARACEST MRI contrast agent to detect enzyme activity. J Am Chem Soc 2006;128:14032–14033.
126. Yoo B, Pagel MD. An overview of responsive MRI contrast agents for molecular imaging. Front Biosci 2008;13:1733–1752.
127. Yoo B, Raam MS, Rosenblum RM, Pagel MD. Enzyme-responsive PARACEST MRI contrast agents: a new biomedical imaging approach for studies of the proteasome. Contrast Media Mol Imaging 2007;2:189–198.
128. Gilad AA, McMahon MT, Walczak P, Winnard PT, Jr, Raman V, van Laarhoven HW, Skoglund CM, Bulte JW, van Zijl PC. Artificial reporter gene providing MRI contrast based on proton exchange. Nat Biotechnol 2007;25:217–219.
129. Liu G, Moake MM, Gilad AA, Jamil M, Har-el Y-E, Long C, Walczak P, Zhang J, Cardona A, DeLiso MA, Sgouros G, Bulte JW, van Zijl PC, McMahon MT. Multi-color in vivo MR imaging of lymph nodes usng DIACEST liposomes. In: Proceedings of the 18th Annual Meeting of ISMRM, Stockholm, Sweden 2010. p 454.
130. McMahon MT, Gilad AA, DeLiso MA, Berman SM, Bulte JW, van Zijl PC. New "multicolor" polypeptide diamagnetic chemical exchange saturation transfer (DIACEST) contrast agents for MRI. Magn Reson Med 2008;60:803–812.
131. Aime S, Castelli DD, Crich SG, Gianolio E, Terreno E. Pushing the sensitivity envelope of lanthanide-based magnetic resonance imaging (MRI) contrast agents for molecular imaging applications. Acc Chem Res 2009;42:822–831.
132. Dagher AP, Aletras A, Choyke P, Balaban RS. Imaging of urea using chemical exchange-dependent saturation transfer at 1.5T. J Magn Reson Imaging 2000;12:745–748.
133. Zhou J, Tryggestad E, Wen Z, Lal B, Zhou T, Grossman R, Wang S, Yan K, Fu D-X, Ford E, Tyler B, Blakeley J, Laterra J, van Zijl PC. Differentiation between glioma and radiation necrosis using molecular magnetic resonance imaging of endogenous proteins and peptides. Nature Med 2011;17:130–134.
134. Dula AN, Dortch RD, Landman BA, Pawate S, Lavin PJ, Welch EB, Gore JC, Smith SA. Application of CEST imaging to study amide proton transfer (APT) in healthy controls and multiple sclerosis pathology at 7 Tesla. In: Proceedings of the 18th Annual Meeting of ISMRM, Stockholm, Sweden 2010. p 4311.
135. Cai K, Haris M, Singh A, Gaddam S, Daye D, Grasley K, II GZ, Hariharan H, Reddy R. Assessment of chemical exchange saturation transfer effects in liver tissue at 7T. In: Proceedings of the 18th Annual Meeting of ISMRM, Stockholm, Sweden 2010. p 2588.
136. Al-Radaideh A, Mougin O, Lim S-Y, Tench C, Constantinescu C, Gowland P. Magnetization transfer (MT) and endogenous chemical exchange saturation transfer (CEST) effects in patients with clinically isolated syndrome. In: Proceedings of the 18th Annual Meeting of ISMRM, Stockholm, Sweden 2010. p 4310.
137. Gilad AA, Winnard PT, Jr, van Zijl PC, Bulte JW. Developing MR reporter genes: promises and pitfalls. NMR Biomed 2007;20:275–290.
136. Chan KW, Liu G, Arifin DR, Bulte JW, McMahon MT. Remote MR sensing of pH and cell viability using LipoCEST-filled microcapsules. In: Proceedings of the 18th Annual Meeting of ISMRM, Stockholm, Sweden 2010. p 1889.
139. Arifin DR, Chan KW, Liu G, Cardona A, Jamil M, Bulte JW, McMahon MT. Remote MRI sensing of pH and cell viability using immunoprotective microcapsules crosslinked with polycationic DIACEST peptides. In: Proceedings of the 18th Annual Meeting of ISMRM, Stockholm, Sweden 2010. p 42.
140. Pasha A, Tircso G, Benyo ET, Brucher E, Sherry AD. Synthesis and characterization of DOTA-(amide)(4) derivatives: equilibrium and kinetic behavior of their lanthanide(III) complexes. Eur J Inorg Chem 2007:4340–4349.
141. Sherry AD, Caravan P, Lenkinski RE. Primer on gadolinium chemistry. J Magn Reson Imaging 2009;30:1240–1248.
142. Li AX, Suchy M, Li C, Poppe C, Gati J, Meakin S, Hudson RH, Menon RS, Bartha M. In vivo detection of a PARACEST agent in mouse brain tumors. In: Proceedings of the 18th Annual Meeting of ISMRM, Stockholm, Sweden 2010. p 3752.
143. Jones CK, Li AX, Suchy M, Hudson RH, Menon RS, Bartha R. In vivo detection of PARACEST agents with relaxation correction. Magn Reson Med 2010;63:1184–1192.
144. Soesbe TC, Rojas-Quijano FA, Merritt ME, Sherry AD. Eu^{3+}-based PARACEST agents with intermediate water exchange rates also act as T_2 exchange (T_{2exch}) contrast agents. In: Proceedings of the 18th Annual Meeting of ISMRM, Stockholm, Sweden 2010. p 39.
145. Ren J, Trokowski R, Zhang S, Malloy CR, Sherry AD. Imaging the tissue distribution of glucose in livers using a PARACEST sensor. Magn Reson Med 2008;60:1047–1055.
146. Wu Y, Zhou Y, Ouari O, Woods M, Zhao P, Soesbe TC, Kiefer GE, Sherry AD. Polymeric PARACEST agents for enhancing MRI contrast sensitivity. J Am Chem Soc 2008;130:13854–13855.